



HAL
open science

Convergence and stability of a high-order leap-frog based discontinuous Galerkin method for the Maxwell equations on non-conforming meshes

Hassan Fahs, Stephane Lanteri

► **To cite this version:**

Hassan Fahs, Stephane Lanteri. Convergence and stability of a high-order leap-frog based discontinuous Galerkin method for the Maxwell equations on non-conforming meshes. [Research Report] RR-6699, INRIA. 2008, pp.27. inria-00332277

HAL Id: inria-00332277

<https://inria.hal.science/inria-00332277>

Submitted on 20 Oct 2008

HAL is a multi-disciplinary open access archive for the deposit and dissemination of scientific research documents, whether they are published or not. The documents may come from teaching and research institutions in France or abroad, or from public or private research centers.

L'archive ouverte pluridisciplinaire **HAL**, est destinée au dépôt et à la diffusion de documents scientifiques de niveau recherche, publiés ou non, émanant des établissements d'enseignement et de recherche français ou étrangers, des laboratoires publics ou privés.



INSTITUT NATIONAL DE RECHERCHE EN INFORMATIQUE ET EN AUTOMATIQUE

*Convergence and stability of a high-order leap-frog
based discontinuous Galerkin method for the
Maxwell equations on non-conforming meshes*

Hassan Fahs — Stéphane Lanteri

N° 6699

October 2008

Thème NUM

 *rapport
de recherche*

Convergence and stability of a high-order leap-frog based discontinuous Galerkin method for the Maxwell equations on non-conforming meshes

Hassan Fahs^{*†}, Stéphane Lanteri[‡]

Thème NUM — Systèmes numériques
Équipes-Projets Nachos

Rapport de recherche n° 6699 — October 2008 — 27 pages

Abstract: In this work, we discuss the formulation, stability, convergence and numerical validation of a high-order leap-frog based non-dissipative discontinuous Galerkin time-domain (DGTD) method for solving Maxwell's equations on non-conforming simplicial meshes. This DGTD method makes use of a nodal polynomial interpolation method for the approximation of the electromagnetic field within a simplex, and of a centered scheme for the calculation of the numerical flux at an interface between neighboring elements. Moreover, the interpolation degree is defined at the element level and the mesh is refined locally in a non-conforming way resulting in arbitrary level hanging nodes. The method is proved to be stable and conserves a discrete analog of the electromagnetic energy for metallic cavities. The convergence of the semi-discrete approximation to Maxwell's equations is established rigorously and bounds on the global divergence error are provided. Numerical experiments with high-order elements show the potential of the method.

Key-words: time-domain Maxwell's equations, discontinuous Galerkin method, leap-frog time scheme, non-conforming meshes

* Corresponding author

† Hassan.Fahs@inria.fr

‡ Stephane.Lanteri@inria.fr

Convergence et stabilité d'une méthode Galerkin discontinue basée sur un schéma saute-mouton d'ordre élevé pour la résolution des équations de Maxwell en maillage non-conformes

Résumé : Nous étudions dans ce rapport la stabilité et la convergence d'une méthode Galerkin discontinue d'ordre élevé pour la résolution des équations de Maxwell en domaine temporel en maillages non-conformes. La méthode repose sur des fonctions de base nodales pour approcher le champ électromagnétique dans un simplexe, un schéma centré pour calculer les flux sur les interfaces entre éléments voisins du maillage et un schéma saute-mouton d'ordre élevé pour l'intégration temporelle. De plus, l'ordre d'interpolation est défini au niveau d'un élément et le maillage est raffiné d'une manière non-conforme autorisant un nombre arbitraire de nœuds flottants. On prouve que la méthode est stable sous une condition de type CFL et qu'un équivalent discret de l'énergie électromagnétique est exactement conservée. On réalise aussi une étude de convergence *hp a priori* ainsi qu'une étude de convergence de l'erreur sur la divergence. Des résultats numériques pour des ordres élevés montrent le potentiel de la méthode.

Mots-clés : équations de Maxwell, domaine temporel, méthode Galerkin discontinue, schéma saute-mouton, maillages non-conformes,

1 Introduction

Time domain solutions of Maxwell's equations find applications in the applied sciences and engineering problems such as the design and optimization of antennas and radars, the design of emerging technologies (high speed electronics, integrated optics, etc.), the study of human exposure to electromagnetic waves [5], to name a few. These problems require high fidelity approximate solutions with a rigorous control of the numerical errors. Even for linear problems such conditions force one to look beyond standard computational techniques and seek new numerical frameworks enabling the accurate, efficient, and robust modeling of wave phenomena over long simulation times in settings of realistic geometrical complexity.

Recently, discontinuous Galerkin methods have attracted much research to solve electromagnetic wave propagation problems. Being higher order versions of traditional finite volume methods [15], discontinuous Galerkin time-domain (DGTD) methods based on discontinuous finite element spaces, easily handle elements of various types and shapes, irregular non-conforming meshes [8]-[9], and even locally varying polynomial degree. They hence offer great flexibility in the mesh design, but also lead to (block-) diagonal mass matrices and therefore yield fully explicit, inherently parallel methods when coupled with explicit time stepping [2]. Moreover, continuity is weakly enforced across mesh interfaces by adding suitable bilinear forms (so-called numerical fluxes) to the standard variational formulations. Whereas high-order discontinuous Galerkin time-domain methods have been developed on conforming hexahedral [6] and tetrahedral [14] meshes, the design of non-conforming discontinuous Galerkin time-domain methods is still in its infancy. In practice, the non-conformity can result from a local refinement of the mesh (*i.e.* h -refinement), of the interpolation degree (*i.e.* p -enrichment) or of both of them (*i.e.* hp -refinement).

This work is concerned with the study of high-order leap-frog schemes that are extensions of the second-order leap-frog scheme adopted in the DGTD methods that are studied in [7]-[8]-[9]-[10]-[11]-[12]. The motivation behind this study is to improve the overall accuracy for the same mesh resolution and/or to improve convergence when the mesh resolution is increased. Not surprisingly, the arbitrary high-order DGTD methods discussed in this work are consistently more accurate than the DGTD methods based on the second-order leap-frog scheme. The high-order leap-frog schemes require more computational operations to update a cell. Fortunately, this can be alleviated by the ability to use discretization meshes with fewer points per wavelength for the same level of accuracy.

The high-order leap-frog schemes considered in this work were initially proposed by Young [25], and further studied by Spachmann *et al.* [22]. The chief attributes of these integrators are that the memory requirements are small and the algorithmic complexity is not significantly increased, with respect to the second-order leap-frog scheme. In the case of Fang's approach [13]-[23], high-order temporal derivatives are replaced with high-order mixed spatial derivatives. Although the memory requirements of Fang's approach are the same as the one of the second-order leap-frog scheme, the resulting scheme is far too complex to implement for most practical problems. One can note here that to our knowledge, these high-order leap-frog schemes have not been used yet in the context of the Maxwell's equations discretized by a discontinuous Galerkin method.

The existing high-order discontinuous Galerkin methods are mostly based on high-order Runge-Kutta (RK) schemes. The low storage RK schemes introduced in [3] are among the most popular choices for time integration of the DG space-discretized Maxwell equations. High-order RKDG schemes have been used by Monk and Richter [18] for solving linear symmetric hyperbolic problems, Hesthaven and Warburton [15], Chen *et al.* [4] and Lu *et al.* [17] for solving time-domain electromagnetics. A dispersion and dissipation study for a high-order DG method for solving Maxwell's equations have been conducted in [20] using several high-order RK schemes. Recently, Kanevsky *et al.* [16] have applied a hybrid implicit-explicit high-order RK scheme to DG methods for solving conservation laws.

This report is structured as follows. In Sec. 2, we introduce the high-order non-conforming DGTD method for solving the system of Maxwell equations. Our two main results, the stability and the hp -convergence of the proposed method, are stated and proved in Sec. 3. In this section we also

establish bounds on the behavior of the divergence error. In Sec. 4 we verify our theoretical results through numerical experiments. Finally, some concluding remarks are presented in Sec. 5.

2 An arbitrary high-order non-conforming DGTD method

We consider the Maxwell equations in three space dimensions for heterogeneous anisotropic linear media with no source. The electric permittivity tensor $\bar{\epsilon}(x)$ and the magnetic permeability tensor $\bar{\mu}(x)$ are varying in space, time-invariant and both symmetric positive definite. The electric field $\vec{E} = {}^t(E_x, E_y, E_z)$ and the magnetic field $\vec{H} = {}^t(H_x, H_y, H_z)$ verify:

$$\begin{cases} \bar{\epsilon} \partial_t \vec{E} &= \text{curl} \vec{H}, \\ \bar{\mu} \partial_t \vec{H} &= -\text{curl} \vec{E}, \end{cases} \quad (1)$$

where the symbol ∂t denotes a time derivative. These equations are set and solved on a bounded polyhedral domain Ω of \mathbb{R}^3 . For the sake of simplicity, a metallic boundary condition is set everywhere on the domain boundary $\partial\Omega$, *i.e.* $\vec{n} \times \vec{E} = 0$ (where \vec{n} denotes the unitary outwards normal).

2.1 Space discretization

We consider a partition Ω_h of Ω into a set of tetrahedra τ_i of size h_i with boundaries $\partial\tau_i$ such that $h = \max_{\tau_i \in \Omega_h} h_i$. To each $\tau_i \in \Omega_h$ we assign an integer $p_i \geq 0$ (the local interpolation degree) and we collect the p_i in the vector $p = \{p_i : \tau_i \in \Omega_h\}$. Of course, if p_i is uniform in all element τ_i of the mesh, we have $p = p_i$. Within this construction we admit meshes with possibly hanging nodes *i.e.* by allowing non-conforming (or irregular) meshes where element vertices can lie in the interior of faces of other elements. However, we assume that the local mesh sizes and approximation degrees are of bounded variation, that is, there exist a constant $\kappa_1 > 0$, depending only on the shape-regularity of the mesh, and a constant $\kappa_2 > 0$, such that:

$$\begin{aligned} \kappa_1^{-1} h_i &\leq h_k \leq \kappa_1 h_i, \\ \kappa_2^{-1} p_i &\leq p_k \leq \kappa_2 p_i, \end{aligned} \quad (2)$$

for all neighboring elements τ_i and τ_k in Ω_h . Nevertheless, the above hypothesis is not restrictive in practice and allows, in particular for geometric refinement and linearly increasing approximation degrees. We also assume that Ω_h is shape regular in the sense that there is a constant $\eta > 0$ such that:

$$\forall \tau_i \in \Omega_h, \quad \frac{h_i}{\rho_i} \leq \eta, \quad (3)$$

where ρ_i is the diameter of the insphere of τ_i . Each tetrahedron τ_i is assumed to be the image, under a smooth bijective (diffeomorphic) mapping, of a fixed reference tetrahedron $\hat{\tau} = \{\hat{x}, \hat{y}, \hat{z} \mid \hat{x}, \hat{y}, \hat{z} \geq 0; \hat{x} + \hat{y} + \hat{z} \leq 1\}$. Assuming that τ_i is a straight faced tetrahedron defined through the coordinates of the four vertices v_1^i, v_2^i, v_3^i and v_4^i (see Fig. 1), the correspondence between the two tetrahedra $\hat{\tau}$ and τ_i is established through the use of the barycentric coordinates $(\lambda_1, \lambda_2, \lambda_3, \lambda_4)$. We recall that any point $\mathbf{x}^i \in \tau_i$ can be expressed as a convex combination of the vertices of τ_i and the mapping is simply given by $\chi_i : (\hat{x}, \hat{y}, \hat{z}) \in \hat{\tau} \rightarrow \mathbf{x}^i$, such that: $\mathbf{x}^i(\hat{x}, \hat{y}, \hat{z}) = \lambda_1 v_1^i + \lambda_2 v_2^i + \lambda_3 v_3^i + \lambda_4 v_4^i$, where $\lambda_1 + \lambda_2 + \lambda_3 + \lambda_4 = 1$ and $0 \leq (\lambda_1, \lambda_2, \lambda_3, \lambda_4) \leq 1$ with $\lambda_1 = 1 - \hat{x} - \hat{y} - \hat{z}$, $\lambda_2 = \hat{x}$, $\lambda_3 = \hat{y}$ and $\lambda_4 = \hat{z}$. For each τ_i , V_i denotes its volume, and $\bar{\epsilon}_i$ and $\bar{\mu}_i$ are respectively the local electric permittivity and magnetic permeability tensors of the medium, which could be varying inside the element τ_i . For two distinct tetrahedra τ_i and τ_k in Ω_h , the intersection $\tau_i \cap \tau_k$ is an (oriented) triangle a_{ik} which we will call interface. For each internal interface a_{ik} , we denote by S_{ik} the measure of a_{ik} and by \vec{n}_{ik} the unitary normal vector, oriented from τ_i towards τ_k . For the boundary interfaces, the index k corresponds to a fictitious element outside the domain. We denote by \mathcal{F}_h^I the union of all interior

faces of Ω_h , by \mathcal{F}_h^B the union of all boundary faces of Ω_h , and by $\mathcal{F}_h = \mathcal{F}_h^I \cap \mathcal{F}_h^B$. Furthermore, we identify \mathcal{F}_h^B to $\partial\Omega$ since Ω is a polyhedron. Finally, we denote by \mathcal{V}_i the set of indices of the elements which are neighbors of τ_i (having an interface in common). We also define the perimeter P_i of τ_i by $P_i = \sum_{k \in \mathcal{V}_i} S_{ik}$. We have the following geometrical property for all elements: $\sum_{k \in \mathcal{V}_i} S_{ik} \vec{n}_{ik} = 0$.

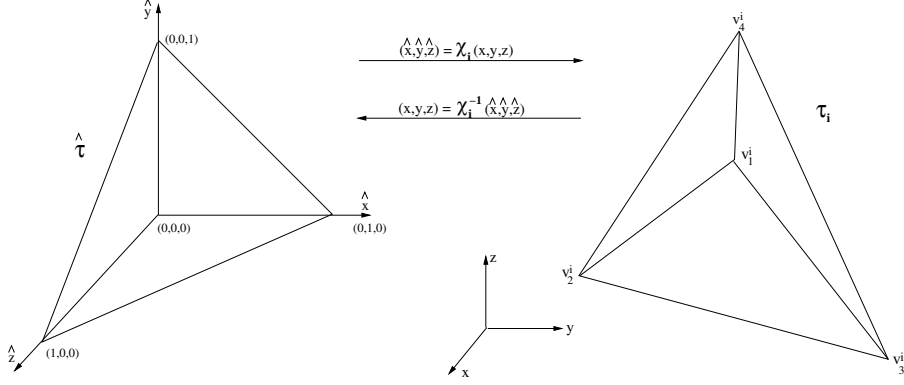


Figure 1: Mapping between the physical tetrahedron τ_i and the reference tetrahedron $\hat{\tau}$.

In the following, for a given partition Ω_h and for a vector p , we seek approximate solutions to (1) in the finite dimensional subspace $V_p(\Omega_h) = \{\vec{v} \in L^2(\Omega)^3 : \vec{v}|_{\tau_i} \in \mathbb{P}_{p_i}(\tau_i), \forall \tau_i \in \Omega_h\}$, where $\mathbb{P}_{p_i}(\tau_i)$ denotes the space of nodal polynomials of degree at most p_i inside the element τ_i . Note that the polynomial degree p_i may vary from element to element in the mesh. By non-conforming interface we mean an interface a_{ik} which is such that at least one of its vertices is a hanging node, or/and such that $p_{i|a_{ik}} \neq p_{k|a_{ik}}$.

Following the discontinuous Galerkin approach, the electric and magnetic fields inside each finite element are sought for as linear combinations $(\vec{\mathbf{E}}_i, \vec{\mathbf{H}}_i)$ of linearly independent basis vector fields $\vec{\varphi}_{ij}$, $1 \leq j \leq d_i$, where d_i denotes the local number of degrees of freedom (DOF) inside τ_i . We denote by $\mathcal{P}_i = \text{Span}(\vec{\varphi}_{ij}, 1 \leq j \leq d_i)$. The approximate fields $(\vec{\mathbf{E}}_h, \vec{\mathbf{H}}_h)$, defined by $(\forall i, \vec{\mathbf{E}}_h|_{\tau_i} = \vec{\mathbf{E}}_i, \vec{\mathbf{H}}_h|_{\tau_i} = \vec{\mathbf{H}}_i)$ are allowed to be completely discontinuous across element boundaries. For such a discontinuous field $\vec{\mathbf{U}}_h$, we define its average $\{\vec{\mathbf{U}}_h\}_{ik}$ through any internal interface a_{ik} , as $\{\vec{\mathbf{U}}_h\}_{ik} = (\vec{\mathbf{U}}_{i|a_{ik}} + \vec{\mathbf{U}}_{k|a_{ik}})/2$. Note that for any internal interface a_{ik} , $\{\vec{\mathbf{U}}_h\}_{ki} = \{\vec{\mathbf{U}}_h\}_{ik}$. Because of this discontinuity, a global variational formulation cannot be obtained. However, dot-multiplying (1) by any given vector function $\vec{\varphi} \in \mathcal{P}_i$, integrating over each single element τ_i and integrating by parts, yields:

$$\begin{cases} \int_{\tau_i} \vec{\varphi} \cdot \bar{\epsilon}_i \partial_t \vec{\mathbf{E}} &= \int_{\tau_i} \text{curl} \vec{\varphi} \cdot \vec{\mathbf{H}} - \int_{\partial\tau_i} \vec{\varphi} \cdot (\vec{\mathbf{H}} \times \vec{n}), \\ \int_{\tau_i} \vec{\varphi} \cdot \bar{\mu}_i \partial_t \vec{\mathbf{H}} &= - \int_{\tau_i} \text{curl} \vec{\varphi} \cdot \vec{\mathbf{E}} + \int_{\partial\tau_i} \vec{\varphi} \cdot (\vec{\mathbf{E}} \times \vec{n}). \end{cases} \quad (4)$$

In Eq. (4), we now replace the exact fields $\vec{\mathbf{E}}$ and $\vec{\mathbf{H}}$ by the approximate fields $\vec{\mathbf{E}}_h$ and $\vec{\mathbf{H}}_h$ in order to evaluate volume integrals. For integrals over $\partial\tau_i$, a specific treatment must be introduced since the approximate fields are discontinuous through element faces. We choose to use a fully centered numerical flux, *i.e.* $\forall i, \forall k \in \mathcal{V}_i, \vec{\mathbf{E}}_{i|a_{ik}} \simeq \{\vec{\mathbf{E}}_h\}_{ik}, \vec{\mathbf{H}}_{i|a_{ik}} \simeq \{\vec{\mathbf{H}}_h\}_{ik}$. The metallic boundary condition on a boundary interface a_{ik} (where k is the element index of a fictitious neighboring element) is dealt with *weakly*, in the sense that traces of fictitious fields $\vec{\mathbf{E}}_k$ and $\vec{\mathbf{H}}_k$ are used for the computation of numerical fluxes for the boundary element τ_i . In the present case, where all boundaries are metallic, we simply take $\vec{\mathbf{E}}_{k|a_{ik}} = -\vec{\mathbf{E}}_{i|a_{ik}}$ and $\vec{\mathbf{H}}_{k|a_{ik}} = \vec{\mathbf{H}}_{i|a_{ik}}$. Replacing surface integrals using the centered numerical flux in (4) and re-integrating by parts yields:

$$\begin{cases} \int_{\tau_i} \vec{\varphi} \cdot \bar{\epsilon}_i \partial_t \vec{\mathbf{E}}_i &= \frac{1}{2} \int_{\tau_i} (\text{curl} \vec{\varphi} \cdot \vec{\mathbf{H}}_i + \text{curl} \vec{\mathbf{H}}_i \cdot \vec{\varphi}) - \frac{1}{2} \sum_{k \in \mathcal{V}_i} \int_{a_{ik}} \vec{\varphi} \cdot (\vec{\mathbf{H}}_k \times \vec{n}_{ik}), \\ \int_{\tau_i} \vec{\varphi} \cdot \bar{\mu}_i \partial_t \vec{\mathbf{H}}_i &= -\frac{1}{2} \int_{\tau_i} (\text{curl} \vec{\varphi} \cdot \vec{\mathbf{E}}_i + \text{curl} \vec{\mathbf{E}}_i \cdot \vec{\varphi}) + \frac{1}{2} \sum_{k \in \mathcal{V}_i} \int_{a_{ik}} \vec{\varphi} \cdot (\vec{\mathbf{E}}_k \times \vec{n}_{ik}). \end{cases} \quad (5)$$

We can rewrite this formulation in terms of scalar unknowns. Inside each element, the fields being recomposed according to $\vec{\mathbf{E}}_i = \sum_{1 \leq j \leq d_i} E_{ij} \vec{\varphi}_{ij}$ and $\vec{\mathbf{H}}_i = \sum_{1 \leq j \leq d_i} H_{ij} \vec{\varphi}_{ij}$. Let us denote by \mathbf{E}_i and \mathbf{H}_i respectively the column vectors $(E_{il})_{1 \leq l \leq d_i}$ and $(H_{il})_{1 \leq l \leq d_i}$. Eq. (5) can be rewritten as:

$$\begin{cases} M_i^\epsilon \partial_t \mathbf{E}_i &= K_i \mathbf{H}_i - \sum_{k \in \mathcal{V}_i} S_{ik} \mathbf{H}_k, \\ M_i^\mu \partial_t \mathbf{H}_i &= -K_i \mathbf{E}_i + \sum_{k \in \mathcal{V}_i} S_{ik} \mathbf{E}_k, \end{cases} \quad (6)$$

where the symmetric positive definite mass matrices M_i^σ (σ stands for ϵ or μ) and the symmetric stiffness matrix K_i (all of size $d_i \times d_i$) are given by :

$$\begin{aligned} (M_i^\sigma)_{jl} &= \int_{\tau_i} {}^t \vec{\varphi}_{ij} \cdot \bar{\sigma}_i \vec{\varphi}_{il}, \\ (K_i)_{jl} &= \frac{1}{2} \int_{\tau_i} {}^t \vec{\varphi}_{ij} \cdot \text{curl} \vec{\varphi}_{il} + {}^t \vec{\varphi}_{il} \cdot \text{curl} \vec{\varphi}_{ij}. \end{aligned}$$

For any interface a_{ik} , the $d_i \times d_k$ rectangular matrix S_{ik} is given by:

$$(S_{ik})_{jl} = \frac{1}{2} \int_{a_{ik}} {}^t \vec{\varphi}_{ij} \cdot (\vec{\varphi}_{kl} \times \vec{n}_{ik}), \quad 1 \leq j \leq d_i, \quad 1 \leq l \leq d_k. \quad (7)$$

2.2 Time discretization

The choice of the time discretization is a crucial step for the global efficiency of the numerical method. The temporal integration methods are divided into two major families: implicit and explicit schemes. Implicit schemes require the solution of large matrix systems resulting in a high computational effort per time step. The quality of the scheme depends strongly on the efficiency of the used linear system solver. The advantage of implicit schemes is their flexibility regarding the choice of the time step since usually, these time schemes are unconditionally stable. Thus, an analysis requires only a small number of solver runs but every time step is burdened by a high numerical effort. Explicit schemes in contrast are easy to implement, produce greater accuracy with less computational effort than implicit methods, but are restricted by a stability criterion enforcing a close linkage of the time step to the spatial discretization parameter. This restriction may result in a large number of iterations per analysis, each iteration with a low computational effort. In this study, we focus on explicit time integration schemes and our objective is to design an arbitrary high-order DGTD method which combines the spatial discretization features of the methods discussed in [8]-[9]-[11], with a family of high-order explicit leap-frog schemes.

The ordinary differential system (5) can be formally seen as a system of the form (see Sec. 3.1 for more details):

$$\begin{cases} \mathbf{M} \partial_t \mathbf{E} &= \mathbf{U} \mathbf{H}, \\ \mathbf{N} \partial_t \mathbf{H} &= \mathbf{V} \mathbf{E}. \end{cases} \quad (8)$$

The one-step explicit time integration methods like Runge-Kutta or leap-frog schemes imply the convenience of storing just one old solution followed by a single update step. Therefore, they are

computationally efficient per update cycle and easy to implement. Moreover, the leap-frog scheme has the advantage to be free of time dissipation. We can introduce the N th-order explicit leap-frog (LF $_N$) integrator as an approximation of the solution of the first-order ODE:

$$\dot{y}(t) = Ay(t) \Rightarrow y(t) = e^{At}y(t_0), \quad (9)$$

with $y(t_0)$ as initial value. The time discrete equivalent of (9) is given by:

$$y(n\Delta t) = e^{A\Delta t}y((n-1)\Delta t). \quad (10)$$

System (8) can be rewritten as:

$$\partial_t \begin{pmatrix} \mathbf{H} \\ \mathbf{E} \end{pmatrix} = \underbrace{\begin{pmatrix} 0 & \mathbf{N}^{-1}\mathbf{V} \\ \mathbf{M}^{-1}\mathbf{U} & 0 \end{pmatrix}}_{\mathbf{A}} \underbrace{\begin{pmatrix} \mathbf{H} \\ \mathbf{E} \end{pmatrix}}_{\mathbf{Y}(t)}. \quad (11)$$

Note that the system matrix \mathbf{A} depends only on the spatial configuration. Seeking a time discrete solution of (11), a discretization in time with a global time step is introduced. The time discrete solution of the first-order system of ODEs (11) is a discretized version of the exponential solution according to its scalar equivalent (10):

$$\mathbf{Y}(n\Delta t) = \Phi(\Delta t)\mathbf{Y}((n-1)\Delta t), \quad (12)$$

with:

$$\Phi(\Delta t) = \sum_{i=0}^{\infty} \frac{\Delta t^i}{i!} \mathbf{A}^i := e^{\mathbf{A}\Delta t}. \quad (13)$$

Finally, the solution of (11) is written as:

$$\begin{pmatrix} \mathbf{H}(n\Delta t) \\ \mathbf{E}(n\Delta t) \end{pmatrix} = \underbrace{\begin{pmatrix} \Phi_{11} & \Phi_{12} \\ \Phi_{21} & \Phi_{22} \end{pmatrix}}_{\Phi} \underbrace{\begin{pmatrix} \mathbf{H}((n-1)\Delta t) \\ \mathbf{E}((n-1)\Delta t) \end{pmatrix}}_{\mathbf{Y}((n-1)\Delta t)}. \quad (14)$$

Introducing a staggered temporal grid, as in the case of LF schemes, we obtain the general LF update equation:

$$\mathbf{H}^{n+1} = [\Phi_{11}^2 - \Phi_{11}\Phi_{12}\Phi_{22}^{-1}\Phi_{21}]\mathbf{H}^{n-1} + [\Phi_{12} + \Phi_{11}\Phi_{12}\Phi_{22}^{-1}]\mathbf{E}^n, \quad (15a)$$

$$\mathbf{E}^{n+2} = [\Phi_{21} + \Phi_{22}\Phi_{21}\Phi_{11}^{-1}]\mathbf{H}^{n+1} + [\Phi_{22}^2 - \Phi_{22}\Phi_{21}\Phi_{11}^{-1}\Phi_{12}]\mathbf{E}^n, \quad (15b)$$

where the electric field quantities are located at even time steps and magnetic quantities at odd time steps as illustrated on Fig. 2. In the case of a non-conducting material, the relation:

$$[\Phi_{11}^2 - \Phi_{11}\Phi_{12}\Phi_{22}^{-1}\Phi_{21}] = [\Phi_{22}^2 - \Phi_{22}\Phi_{21}\Phi_{11}^{-1}\Phi_{12}] = \mathbf{I} + \mathcal{O}(\Delta t^{N+1}), \quad (16)$$

holds, which is a characteristic of a LF scheme.

In the sequel, superscripts refer to time stations and Δt is the global time step. The unknowns related to the electric field are approximated at integer time-stations $t^n = n\Delta t$ and are denoted by \mathbf{E}_i^n . The unknowns related to the magnetic field are approximated at half-integer time-stations $t^{n+1/2} = (n+1/2)\Delta t$ and are denoted by $\mathbf{H}_i^{n+1/2}$.

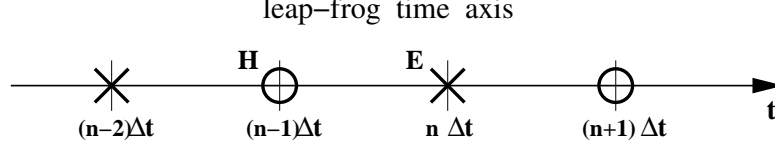


Figure 2: Temporal allocation of electric (\times) and magnetic (\odot) fields in the LF scheme.

Note that here, the used time step Δt is in comparison to the time step defined in (10) twice as large. The LF_N for $N = 2$ and 4 integrators are constructed as follows [25]-[22]:

$$\left\{ \begin{array}{ll} \mathbf{T}_1 = \Delta t (M_i^\epsilon)^{-1} \text{curl} \vec{\mathbf{H}}_i^{n+\frac{1}{2}}, & \mathbf{T}_1^* = -\Delta t (M_i^\mu)^{-1} \text{curl} \vec{\mathbf{E}}_i^{n+1}, \\ \mathbf{T}_2 = -\Delta t (M_i^\mu)^{-1} \text{curl} \mathbf{T}_1, & \mathbf{T}_2^* = \Delta t (M_i^\epsilon)^{-1} \text{curl} \mathbf{T}_1^*, \\ \mathbf{T}_3 = \Delta t (M_i^\epsilon)^{-1} \text{curl} \mathbf{T}_2, & \mathbf{T}_3^* = -\Delta t (M_i^\mu)^{-1} \text{curl} \mathbf{T}_2^*. \\ \\ \text{LF}_2 : \left\{ \begin{array}{l} \mathbf{E}_i^{n+1} = \mathbf{E}_i^n + \mathbf{T}_1, \\ \mathbf{H}_i^{n+\frac{3}{2}} = \mathbf{H}_i^{n+\frac{1}{2}} + \mathbf{T}_1^*. \end{array} \right. & (17) \\ \\ \text{LF}_4 : \left\{ \begin{array}{l} \mathbf{E}_i^{n+1} = \mathbf{E}_i^n + \mathbf{T}_1 + \mathbf{T}_3/24, \\ \mathbf{H}_i^{n+\frac{3}{2}} = \mathbf{H}_i^{n+\frac{1}{2}} + \mathbf{T}_1^* + \mathbf{T}_3^*/24. \end{array} \right. \end{array} \right.$$

Here the \mathbf{T}_i and \mathbf{T}_i^* ($i = 1, 2, 3$) can be combined. Moreover, \mathbf{T}_3 (resp. \mathbf{T}_3^*) is a temporary vector. However, in a practical implementation, this vector is not used since the calculations for \mathbf{T}_3 and $\vec{\mathbf{E}}_i^{n+1}$ (resp. \mathbf{T}_3^* and $\vec{\mathbf{H}}_i^{n+\frac{1}{2}}$) can be combined. Thus, the LF_4 scheme requires 2 times more memory storage and 3 times more arithmetic operations than the LF_2 scheme. In general, the LF_N scheme requires $N/2$ times more memory storage and $(N-1)$ times more arithmetic operations than the LF_2 scheme. A pictorial representation of the extended LF_4 integrator is shown on Fig. 3.

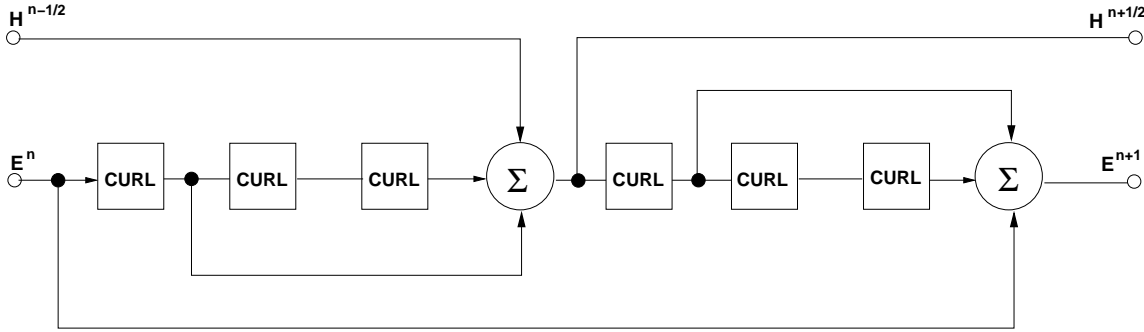


Figure 3: A pictorial representation of the extended LF_4 scheme (multiplicative constants omitted).
Figure taken from [25].

For the treatment of the boundary condition on an interface $a_{ik} \in \mathcal{F}_h^B$, we use:

$$\mathbf{E}_{k|a_{ik}}^n = -\mathbf{E}_{i|a_{ik}}^n \quad \text{and} \quad \mathbf{H}_{k|a_{ik}}^{n+\frac{1}{2}} = -\mathbf{H}_{i|a_{ik}}^{n+\frac{1}{2}} \quad (18)$$

3 Stability and convergence analysis

In this section we study the stability and convergence properties of the high-order discontinuous Galerkin method introduced previously.

3.1 Stability

Here, we aim at giving and proving a sufficient condition for the L^2 -stability of the proposed high-order DGTD method. We use the same kind of energy approach as in [14] where a quadratic form plays the role of a Lyapunov function of the whole set of numerical unknowns. To this end, we suppose that all electric (resp. magnetic) unknowns are gathered in a column vector \mathbb{E} (resp. \mathbb{H}) of size $d = \sum_i d_i$.

Then the space discretized system (6) can be rewritten as:

$$\begin{cases} \mathbb{M}^\epsilon \partial_t \mathbb{E} &= \mathbb{K} \mathbb{H} - \mathbb{A} \mathbb{H} - \mathbb{B} \mathbb{H}, \\ \mathbb{M}^\mu \partial_t \mathbb{H} &= -\mathbb{K} \mathbb{E} + \mathbb{A} \mathbb{E} - \mathbb{B} \mathbb{E}, \end{cases} \quad (19)$$

where we have the following definitions and properties:

- $\mathbb{M}^\epsilon, \mathbb{M}^\mu$ and \mathbb{K} are $d \times d$ block diagonal matrices with diagonal blocks equal to M_i^ϵ, M_i^μ and K_i respectively. Therefore \mathbb{M}^ϵ and \mathbb{M}^μ are symmetric positive definite matrices, and \mathbb{K} is a symmetric matrix.
- \mathbb{A} is also a $d \times d$ block sparse matrix, whose non-zero blocks are equal to S_{ik} when a_{ik} is an internal interface of the mesh. Since $\vec{n}_{ki} = -\vec{n}_{ik}$, it can be checked from (7) that $(S_{ik})_{jl} = (S_{ki})_{lj}$ and then $S_{ki} = {}^t S_{ik}$; thus \mathbb{A} is a symmetric matrix.
- \mathbb{B} is a $d \times d$ block diagonal matrix, whose non-zero blocks are equal to S_{ik} when a_{ik} is a metallic boundary interface of the mesh. In that case, $(S_{ik})_{jl} = -(S_{ik})_{lj}$; thus \mathbb{B} is a skew-symmetric matrix.

The discontinuous Galerkin DGTD- \mathbb{P}_{p_i} method using centered fluxes combined with a N th order leap-frog (LF $_N$) time scheme can be written, using the matrix $\mathbb{S} = \mathbb{K} - \mathbb{A} - \mathbb{B}$, in the general form:

$$\begin{cases} \mathbb{M}^\epsilon \frac{\mathbb{E}^{n+1} - \mathbb{E}^n}{\Delta t} &= \mathbb{S}_N \mathbb{H}^{n+\frac{1}{2}}, \\ \mathbb{M}^\mu \frac{\mathbb{H}^{n+\frac{3}{2}} - \mathbb{H}^{n+\frac{1}{2}}}{\Delta t} &= -{}^t \mathbb{S}_N \mathbb{E}^{n+1}, \end{cases} \quad (20)$$

where the matrix \mathbb{S}_N (N being the order of the leap-frog scheme) verifies:

$$\mathbb{S}_N = \begin{cases} \mathbb{S} & \text{if } N = 2, \\ \mathbb{S} \left(\mathbb{I} - \frac{\Delta t^2}{24} \mathbb{M}^{-\mu} {}^t \mathbb{S} \mathbb{M}^{-\epsilon} \mathbb{S} \right) & \text{if } N = 4, \\ \mathbb{S} \left(\mathbb{I} + \sum_{i=1}^{N/2-1} \frac{(-1)^i}{(2i+1)! 2^{2i}} (\Delta t^2 \mathbb{M}^{-\mu} {}^t \mathbb{S} \mathbb{M}^{-\epsilon} \mathbb{S})^i \right) & \forall N > 2, \text{ even.} \end{cases} \quad (21)$$

We now define the following discrete version of the electromagnetic energy.

Definition 3.1 *We consider the following electromagnetic energies inside each tetrahedron and in the whole domain Ω :*

- *the local energy :* $\forall i, \mathcal{E}_i^n = \frac{1}{2} ({}^t \mathbf{E}_i^n M_i^\epsilon \mathbf{E}_i^n + {}^t \mathbf{H}_i^{n-\frac{1}{2}} M_i^\mu \mathbf{H}_i^{n+\frac{1}{2}}),$ (22)

- *the global energy :* $\mathcal{E}^n = \frac{1}{2} ({}^t \mathbb{E}^n \mathbb{M}^\epsilon \mathbb{E}^n + {}^t \mathbb{H}^{n-\frac{1}{2}} \mathbb{M}^\mu \mathbb{H}^{n+\frac{1}{2}}).$ (23)

In the following, we shall prove that the global energy (23) is conserved through a time step and that it is a positive definite quadratic form of all unknowns under a CFL-like condition on the global time step Δt .

Lemma 3.1 *Using the DGTD- \mathbb{P}_{p_i} method (20)-(21) for solving (1) with metallic boundaries only, the global discrete energy (23) is exactly conserved, i.e. $\mathcal{E}^{n+1} - \mathcal{E}^n = 0$, $\forall n$.*

Proof. We denote by $\mathbb{E}^{n+\frac{1}{2}} = \frac{\mathbb{E}^{n+1} + \mathbb{E}^n}{2}$. We have :

$$\begin{aligned} \mathcal{E}^{n+1} - \mathcal{E}^n &= {}^t\mathbb{E}^{n+\frac{1}{2}}\mathbb{M}^\epsilon(\mathbb{E}^{n+1} - \mathbb{E}^n) + \frac{1}{2}{}^t\mathbb{H}^{n+\frac{1}{2}}\mathbb{M}^\mu(\mathbb{H}^{n+\frac{3}{2}} - \mathbb{H}^{n-\frac{1}{2}}) \\ &= \Delta t {}^t\mathbb{E}^{n+\frac{1}{2}}\mathbb{S}_N\mathbb{H}^{n+\frac{1}{2}} - \frac{1}{2}\Delta t {}^t\mathbb{H}^{n+\frac{1}{2}}({}^t\mathbb{S}_N\mathbb{E}^{n+1} + {}^t\mathbb{S}_N\mathbb{E}^n) \\ &= \Delta t {}^t\mathbb{H}^{n+\frac{1}{2}}({}^t\mathbb{S}_N - {}^t\mathbb{S}_N)\mathbb{E}^{n+\frac{1}{2}} = 0. \end{aligned}$$

This concludes the proof. \square

Lemma 3.2 *Using the DGTD- \mathbb{P}_{p_i} method (20)-(21), the global discrete electromagnetic energy \mathcal{E}^n (23) is a positive definite quadratic form of all unknowns if:*

$$\Delta t \leq \frac{2}{d_N}, \quad \text{with } d_N = \|\mathbb{M}^{-\frac{\mu}{2}} {}^t\mathbb{S}_N \mathbb{M}^{-\frac{\epsilon}{2}}\|, \quad (24)$$

where $\|\cdot\|$ denote the canonical norm of a matrix ($\forall X, \|AX\| \leq \|A\|\|X\|$), and the matrix $\mathbb{M}^{-\frac{\sigma}{2}}$ is the inverse square root of \mathbb{M}^σ . Also, for a given mesh, the stability limit of the LF₄ scheme is roughly 2.85 times larger than that of the LF₂ scheme.

Proof. The mass matrices \mathbb{M}^ϵ and \mathbb{M}^μ are symmetric positive definite and we can construct in a simple way their square root (also symmetric positive definite) denoted by $\mathbb{M}^{\frac{\epsilon}{2}}$ and $\mathbb{M}^{\frac{\mu}{2}}$ respectively. Moreover:

$$\begin{aligned} \mathcal{E}^n &= \frac{1}{2} {}^t\mathbb{E}^n \mathbb{M}^\epsilon \mathbb{E}^n + \frac{1}{2} {}^t\mathbb{H}^{n-\frac{1}{2}} \mathbb{M}^\mu \mathbb{H}^{n+\frac{1}{2}} \\ &= \frac{1}{2} {}^t\mathbb{E}^n \mathbb{M}^\epsilon \mathbb{E}^n + \frac{1}{2} {}^t\mathbb{H}^{n-\frac{1}{2}} \mathbb{M}^\mu \mathbb{H}^{n-\frac{1}{2}} - \frac{\Delta t}{2} {}^t\mathbb{H}^{n-\frac{1}{2}} {}^t\mathbb{S}_N \mathbb{E}^n \\ &\geq \frac{1}{2} \|\mathbb{M}^{\frac{\epsilon}{2}} \mathbb{E}^n\|^2 + \frac{1}{2} \|\mathbb{M}^{\frac{\mu}{2}} \mathbb{H}^{n-\frac{1}{2}}\|^2 - \frac{\Delta t}{2} |{}^t\mathbb{H}^{n-\frac{1}{2}} \mathbb{M}^{\frac{\mu}{2}} \mathbb{M}^{-\frac{\mu}{2}} {}^t\mathbb{S}_N \mathbb{M}^{-\frac{\epsilon}{2}} \mathbb{M}^{\frac{\epsilon}{2}} \mathbb{E}^n| \\ &\geq \frac{1}{2} \|\mathbb{M}^{\frac{\epsilon}{2}} \mathbb{E}^n\|^2 + \frac{1}{2} \|\mathbb{M}^{\frac{\mu}{2}} \mathbb{H}^{n-\frac{1}{2}}\|^2 - \frac{d_N \Delta t}{2} \|\mathbb{M}^{\frac{\mu}{2}} \mathbb{H}^{n-\frac{1}{2}}\| \|\mathbb{M}^{\frac{\epsilon}{2}} \mathbb{E}^n\|. \end{aligned}$$

At this point, we choose to use an upper bound for the term $\|\mathbb{M}^{\frac{\mu}{2}} \mathbb{H}^{n-\frac{1}{2}}\| \|\mathbb{M}^{\frac{\epsilon}{2}} \mathbb{E}^n\|$ which might lead to suboptimal lower bounds for the energy (and then to a slightly too severe stability limit for the DGTD method). Anyway, this stability limit is only sufficient, and not really close to necessary. We use the inequality:

$$\|\mathbb{M}^{\frac{\mu}{2}} \mathbb{H}^{n-\frac{1}{2}}\| \|\mathbb{M}^{\frac{\epsilon}{2}} \mathbb{E}^n\| \leq \frac{1}{2} (\|\mathbb{M}^{\frac{\mu}{2}} \mathbb{H}^{n-\frac{1}{2}}\|^2 + \|\mathbb{M}^{\frac{\epsilon}{2}} \mathbb{E}^n\|^2).$$

We then sum up the lower bounds for \mathcal{E}^n to obtain:

$$\mathcal{E}^n \geq \frac{1}{2} \left(1 - \frac{d_N \Delta t}{2}\right) \|\mathbb{M}^{\frac{\epsilon}{2}} \mathbb{E}^n\|^2 + \frac{1}{2} \left(1 - \frac{d_N \Delta t}{2}\right) \|\mathbb{M}^{\frac{\mu}{2}} \mathbb{H}^{n-\frac{1}{2}}\|^2.$$

Then, under the condition proposed in Lemma 3.2, the electromagnetic energy \mathcal{E}^n is a positive definite quadratic form of all unknowns.

For a given mesh, using the definition (21) of \mathbb{S}_N , the LF₄ scheme is stable if:

$$\begin{aligned}
& \Delta t \|\mathbf{M}^{-\frac{\mu}{2}} {}^t\mathbf{S}_4 \mathbf{M}^{-\frac{\epsilon}{2}}\| && \leq 2, \\
\Rightarrow & \Delta t \|\mathbf{M}^{-\frac{\mu}{2}} (\mathbf{S}_2 - \frac{\Delta t^2}{24} \mathbf{S}_2 \mathbf{M}^{-\mu} {}^t\mathbf{S}_2 \mathbf{M}^{-\epsilon} \mathbf{S}_2) \mathbf{M}^{-\frac{\epsilon}{2}}\| && \leq 2, \\
\Rightarrow & |\Delta t d_2 - \frac{\Delta t^3}{24} d_2^3| && \leq 2.
\end{aligned}$$

This inequality is verified if and only if $d_2 \Delta t \leq 2(\sqrt[3]{2} + \sqrt[3]{4}) \simeq 2(2.847)$. This concludes the proof. \square

Now, we denote by $\nu_N = \text{CFL}_N / \text{CFL}_2$ the ratio between the stability limit of the LF_N scheme and the LF_2 scheme, and by $r_N = \nu_N / (N/2)$ the ratio between ν_N and the additional memory storage between the LF_N and LF_2 schemes. Tab. 1 lists the values of ν_N and r_N for several values of N .

Table 1: *The values of ν_N and r_N for several LF_N schemes.*

N	2	4	6	8	10	12	14	16	18	20
ν_N	1	2.847	3.681	3.793	5.272	4.437	6.422	7.534	7.265	8.909
r_N	1	1.424	1.227	0.948	1.05	0.739	0.917	0.942	0.807	0.891

As it can be seen from Tab. 1, the choice of the LF_4 scheme is advantageous with respect to the r_N ratio.

Now, our objective is to give an explicit CFL condition on Δt under which the local energy (22) is a positive definite quadratic form of the numerical unknowns \mathbf{E}_i^n and $\mathbf{H}_i^{n-\frac{1}{2}}$. We first need some classical definitions.

Definition 3.2 *We assume that the media is isotropic and such that the tensors $\bar{\epsilon}_i$ and $\bar{\mu}_i$ are piecewise constant, i.e. $\bar{\epsilon}_i = \epsilon_i$ and $\bar{\mu}_i = \mu_i$. We denote by $c_i = 1/\sqrt{\epsilon_i \mu_i}$ the propagation speed in the element τ_i . We also assume that there exist dimensionless constants α_i and β_{ik} ($k \in \mathcal{V}_i$) such that:*

$$\forall \vec{\mathbf{X}} \in \mathcal{P}_i, \begin{cases} \|\text{curl} \vec{\mathbf{X}}\|_{\tau_i} \leq \frac{\alpha_i P_i}{V_i} \|\vec{\mathbf{X}}\|_{\tau_i}, \\ \|\vec{\mathbf{X}}\|_{a_{ik}}^2 \leq \frac{\beta_{ik} S_{ik}}{V_i} \|\vec{\mathbf{X}}\|_{\tau_i}^2, \end{cases} \quad (25)$$

where $\|\vec{\mathbf{X}}\|_{\tau_i}$ and $\|\vec{\mathbf{X}}\|_{a_{ik}}$ denote the L^2 -norms of the vector field $\vec{\mathbf{X}}$ over τ_i and the interface a_{ik} respectively.

Lemma 3.3 *Using the scheme (6)-(17)-(18), under assumptions of Definition 3.2, the local discrete energy \mathcal{E}_i^n (22) is a positive definite quadratic form of all unknowns $(\mathbf{E}_i^n, \mathbf{H}_i^{n-\frac{1}{2}})$ and the scheme is stable if the time step Δt is such that:*

$$\forall i, \forall k \in \mathcal{V}_i, \quad c_i \Delta t [2\alpha_i + \beta_{ik}] < \frac{4V_i}{P_i}, \quad (26)$$

(with the convention that, in the above formula, k should be replaced by i for a metallic boundary interface a_{ik}).

Proof. Using the scheme (5) to replace the occurrences of $\mathbf{H}_i^{n+\frac{1}{2}}$ in the definition of \mathcal{E}_i , and using the boundary fluxes given in (18), we get:

$$\begin{aligned}
\mathcal{E}_i^n &= \frac{\epsilon_i}{2} \|\mathbf{E}_i^n\|_{\tau_i}^2 + \frac{\epsilon_i}{2} \|\mathbf{H}_i^{n-\frac{1}{2}}\|_{\tau_i}^2 - \frac{\Delta t}{4} \mathbb{X}_i^n, \quad \text{with} \\
\mathbb{X}_i^n &= \int_{T_i} \left(\text{curl} \vec{\mathbf{H}}_i^{n-\frac{1}{2}} \cdot \vec{\mathbf{E}}_i^n + \text{curl} \vec{\mathbf{E}}_i^n \cdot \vec{\mathbf{H}}_i^{n-\frac{1}{2}} \right) - \sum_{k \in \mathcal{V}_i} \int_{a_{ik}} (\vec{\mathbf{H}}_i^{n-\frac{1}{2}} \times \vec{\mathbf{E}}_k^n) \cdot \vec{n}_{ik}.
\end{aligned}$$

For any metallic or internal interface a_{ik} , we have:

$$\begin{aligned}
\left| \int_{a_{ik}} (\vec{\mathbf{H}}_i^{n-\frac{1}{2}} \times \vec{\mathbf{E}}_k) \cdot \vec{n}_{ik} \right| &\leq \frac{1}{\sqrt{\mu_i \epsilon_i}} \int_{a_{ik}} \|\sqrt{\mu_i} \vec{\mathbf{H}}_i^{n-\frac{1}{2}}\| \|\sqrt{\epsilon_i} \vec{\mathbf{E}}_k^n\| \\
&\leq \frac{1}{2} \sqrt{\frac{\mu_i}{\epsilon_i}} \|\vec{\mathbf{H}}_i^{n-\frac{1}{2}}\|_{a_{ik}}^2 + \frac{1}{2} \sqrt{\frac{\epsilon_i}{\mu_i}} \|\vec{\mathbf{E}}_k^n\|_{a_{ik}}^2 \\
&\leq \frac{1}{2} \sqrt{\frac{\mu_i}{\epsilon_i}} \frac{\beta_{ki} S_{ik}}{V_i} \|\vec{\mathbf{H}}_i^{n-\frac{1}{2}}\|_{\tau_i}^2 + \frac{1}{2} \sqrt{\frac{\epsilon_i}{\mu_i}} \frac{\beta_{ki} S_{ik}}{V_k} \|\vec{\mathbf{E}}_k^n\|_{\tau_i}^2.
\end{aligned}$$

In the remainder of the proof, we omit the superscripts n and $n-1/2$ in the electric and magnetic variables respectively. We have that:

$$\begin{aligned}
|\mathbb{X}_i^n| &\leq \|\operatorname{curl} \vec{\mathbf{H}}_i\|_{\tau_i} \|\vec{\mathbf{E}}_i\|_{\tau_i} + \|\operatorname{curl} \vec{\mathbf{E}}_i\|_{\tau_i} \|\vec{\mathbf{H}}_i\|_{\tau_i} + \frac{1}{2} \sum_{k \in \mathcal{V}_i} \left(\sqrt{\frac{\mu_i}{\epsilon_i}} \|\vec{\mathbf{H}}_i\|_{a_{ik}}^2 + \sqrt{\frac{\epsilon_i}{\mu_i}} \|\vec{\mathbf{E}}_k\|_{a_{ik}}^2 \right) \\
&\leq \frac{2\alpha_i P_i}{V_i} \|\vec{\mathbf{H}}_i\|_{\tau_i} \|\vec{\mathbf{E}}_i\|_{\tau_i} + \frac{1}{2} \sum_{k \in \mathcal{V}_i} \left(\sqrt{\frac{\mu_i}{\epsilon_i}} \frac{\beta_{ki} S_{ik}}{V_i} \|\vec{\mathbf{H}}_i\|_{\tau_i}^2 + \sqrt{\frac{\epsilon_i}{\mu_i}} \frac{\beta_{ki} S_{ik}}{V_k} \|\vec{\mathbf{E}}_k\|_{\tau_i}^2 \right).
\end{aligned}$$

Noticing that $\|\vec{\mathbf{H}}_i\|_{\tau_i} \|\vec{\mathbf{E}}_i\|_{\tau_i} \leq \frac{C_i}{2} (\mu_i \|\vec{\mathbf{H}}_i\|_{\tau_i}^2 + \epsilon_i \|\vec{\mathbf{E}}_i\|_{\tau_i}^2)$, gathering all lower bounds for terms in the expression of \mathcal{E}_i^n and using $P_i = \sum_{k \in \mathcal{V}_i} S_{ik}$ leads to:

$$\begin{aligned}
\mathcal{E}_i^n &\geq \sum_{k \in \mathcal{V}_i} S_{ik} \left(\frac{1}{2P_i} - \frac{\alpha_i C_i \Delta t}{4V_i} \right) (\epsilon_i \|\vec{\mathbf{E}}_i\|_{\tau_i}^2 + \mu_i \|\vec{\mathbf{H}}_i\|_{\tau_i}^2) \\
&\quad - \frac{\Delta t}{8} \sum_{k \in \mathcal{V}_i} S_{ik} \left(\sqrt{\frac{\mu_i}{\epsilon_i}} \frac{\beta_{ik}}{V_i} \|\vec{\mathbf{H}}_i\|_{\tau_i}^2 + \sqrt{\frac{\epsilon_i}{\mu_i}} \frac{\beta_{ki}}{V_k} \|\vec{\mathbf{E}}_k\|_{\tau_i}^2 \right).
\end{aligned}$$

Then, summing up these inequalities in order to obtain a lower bound for $\sum_i \mathcal{E}_i$ leads to an expression that we reorganize using sums over interfaces a_{ik} . We find that $\sum_i \mathcal{E}_i \geq \sum_{a_{ik}} S_{ik} W_{ik}$ with:

$$\begin{aligned}
W_{ik} &= \epsilon_i \|\vec{\mathbf{E}}_i\|_{\tau_i}^2 \left(\frac{1}{2P_i} - \frac{\alpha_i C_i \Delta t}{4V_i} - \frac{\beta_{ik} C_i \Delta t}{8V_i} \right) + \\
&\quad \mu_i \|\vec{\mathbf{H}}_i\|_{\tau_i}^2 \left(\frac{1}{2P_i} - \frac{\alpha_i C_i \Delta t}{4V_i} - \frac{\beta_{ik} C_i \Delta t}{8V_i} \right) + \\
&\quad \epsilon_k \|\vec{\mathbf{E}}_k\|_{\tau_k}^2 \left(\frac{1}{2P_k} - \frac{\alpha_k C_k \Delta t}{4V_k} - \frac{\beta_{ki} C_k \Delta t}{8V_k} \right) + \\
&\quad \mu_k \|\vec{\mathbf{H}}_k\|_{\tau_k}^2 \left(\frac{1}{2P_k} - \frac{\alpha_k C_k \Delta t}{4V_k} - \frac{\beta_{ki} C_k \Delta t}{8V_k} \right).
\end{aligned}$$

Then, under the conditions of Lemma 3.3, W_{ik} is a positive definite quadratic form and the local energy is a positive definite quadratic form of all unknowns. This concludes the proof. \square

Note that, the existence of the constants α_i and β_{ik} ($k \in \mathcal{V}_i$) is always ensured. The values of α_i only depend on the local polynomial order p_i while the values of β_{ik} depend on p_i and on the number of hanging nodes on the interface a_{ik} . For instance, for orthogonal polynomials on a d -simplex $\beta_{ik} = (p_i + 1)(p_i + d)/d$ (see [24]), and for arbitrary basis functions these values are given by:

$$\left(\frac{\alpha_i^2 P_i^2}{V_i^2}; \frac{\beta_{ik} S_{ik}}{V_i}\right) = (\|M^{-1/2} S_1 M^{-1/2}\|; \|M^{-1/2} S_2 M^{-1/2}\|),$$

where M is the mass matrix without material parameter, $S_2 = 2S_{ik}$, and $S_1 = \int_{\tau_i} \text{curl} \vec{\varphi}_{ij} \cdot \text{curl} \vec{\varphi}_{il}$, $1 \leq j, l \leq d_i$. Moreover, the value of β_{ik} verifies the properties of Lemma 2 of [10].

3.2 Convergence

A convergence analysis of the LF₂ based DGTD- \mathbb{P}_{p_i} method is conducted in [14] in the case of conforming simplicial meshes and $p_i = p$ everywhere. In this section, our objective is to obtain an *a priori* error estimates depending on h and p , which establishes the rate of convergence of the proposed hp -like DGTD method.

We consider again the Maxwell problem: find $(\vec{E}, \vec{H}) : \Omega \times]0, T[\rightarrow \mathbb{R}^3 \times \mathbb{R}^3$ such that,

$$\begin{cases} \bar{\epsilon} \partial_t \vec{E} &= \text{curl} \vec{H} & \text{in } \Omega, \\ \bar{\mu} \partial_t \vec{H} &= -\text{curl} \vec{E} & \text{in } \Omega, \end{cases} \quad (27a)$$

$$\begin{cases} \vec{n} \times \vec{E} &= 0 & \text{on } \partial\Omega, \\ \vec{E}(\vec{x}, 0) &= \vec{E}_0(\vec{x}) & \text{in } \Omega, \\ \vec{H}(\vec{x}, 0) &= \vec{H}_0(\vec{x}) & \text{in } \Omega, \end{cases} \quad (27b)$$

$$\begin{cases} \nabla \cdot \vec{E} &= 0 & \text{in } \Omega, \\ \nabla \cdot \vec{H} &= 0 & \text{in } \Omega. \end{cases} \quad (27c)$$

We assume that $\bar{\epsilon}, \bar{\mu} \in [L^\infty(\Omega)]^{3 \times 3}$ and $\exists C_1, C_2 > 0$ such that:

$$\forall \vec{\xi} \in \mathbb{R}^3 : \begin{cases} C_1 |\vec{\xi}|^2 \leq \bar{\epsilon} \vec{\xi} \cdot \vec{\xi} \leq C_2 |\vec{\xi}|^2, \\ C_1 |\vec{\xi}|^2 \leq \bar{\mu} \vec{\xi} \cdot \vec{\xi} \leq C_2 |\vec{\xi}|^2. \end{cases} \quad (28)$$

The problem (27) admits a unique solution $(\vec{E}, \vec{H}) \in [C^1(0, T; [L^2(\Omega)]^3) \cap C^0(0, T; H_0(\text{curl}, \Omega))]^2$ (see [19] for more details), where $H_0(\text{curl}, \Omega) = \{\vec{u} \in H(\text{curl}, \Omega) \text{ such that } \vec{n} \times \vec{u} = 0\}$.

For a real $s \geq 0$, we define the classical broken space :

$$H^s(\Omega_h) = \{v \in L^2(\Omega) : \forall \tau_i \in \Omega_h, v|_{\tau_i} \in H^s(\tau_i)\}. \quad (29)$$

The space $H^s(\Omega_h)$ is equipped with the natural norm, for $v \in H^s(\Omega_h)$:

$$\|v\|_{s,h} = \left(\sum_{\tau_i \in \Omega_h} \|v\|_{s,\tau_i}^2 \right)^{\frac{1}{2}}, \quad (30)$$

where $\|\cdot\|_{s,\tau_i}$ is the usual Sobolev norm of H^s on τ_i . For $s > \frac{1}{2}$, the elementwise traces of functions in $H^s(\Omega_h)$ belongs to $tr(\mathcal{F}_h) = \Pi_{\tau_i \in \Omega_h} L^2(\partial\tau_i)$. We denote by $\mathbf{H}^s(\Omega_h)$ the vectorial broken space $[H^s(\Omega_h)]^3$ and the associated norm defined by :

$$\|\vec{v}\|_{s,h} = \left(\sum_{j=1}^3 \|v_j\|_{s,h}^2 \right)^{\frac{1}{2}}, \quad (31)$$

where $\vec{v} = (v_1, v_2, v_3) \in \mathbf{H}^s(\Omega_h)$. We define the jump of a function $\vec{v} \in \mathbf{H}^s(\Omega_h)$:

$$\begin{aligned} \forall a_{ik} \in \mathcal{F}_h^I, \quad \llbracket \vec{v} \rrbracket_{ik}^i &= \llbracket \vec{v} \rrbracket_{a_{ik}}^{\tau_i} = (\vec{v}_k|_{a_{ik}} - \vec{v}_i|_{a_{ik}}) \times \vec{n}_{ik}, \\ \forall a_{ik} \in \mathcal{F}_h^B, \quad \llbracket \vec{v} \rrbracket_{ik}^i &= -\vec{v}_i|_{a_{ik}} \times \vec{n}_{ik}. \end{aligned} \quad (32)$$

We associate to the continuous problem (27a) the following space discretized problem: find $(\vec{\mathbf{E}}(\cdot, t), \vec{\mathbf{H}}(\cdot, t)) \in \mathbf{H}^1(\Omega_h) \times \mathbf{H}^1(\Omega_h)$ such that, $\forall \tau_i \in \Omega_h$ and $\forall \vec{\phi}, \vec{\psi} \in \mathbf{H}^1(\Omega_h)$,

$$\left\{ \begin{aligned} \int_{\tau_i} \vec{\phi}_i \cdot \bar{\epsilon}_i \partial_t \vec{\mathbf{E}}_i - \int_{\tau_i} \vec{\mathbf{H}}_i \cdot \text{curl} \vec{\phi}_i &+ \sum_{\substack{k \in \mathcal{V}_i^I \\ a_{ik} \in \mathcal{F}_h^I}} \int_{a_{ik}} \vec{\phi}_i \cdot (\vec{\mathbf{H}}|_{a_{ik}} \times \vec{n}_{ik}) \\ &+ \sum_{\substack{k \in \mathcal{V}_i^B \\ a_{ik} \in \mathcal{F}_h^B}} \int_{a_{ik}} \vec{\phi}_i \cdot (\vec{\mathbf{H}}|_{a_{ik}} \times \vec{n}_{ik}) = 0, \\ \int_{\tau_i} \vec{\psi}_i \cdot \bar{\mu}_i \partial_t \vec{\mathbf{H}}_i + \int_{\tau_i} \vec{\mathbf{E}}_i \cdot \text{curl} \vec{\psi}_i &- \sum_{\substack{k \in \mathcal{V}_i^I \\ a_{ik} \in \mathcal{F}_h^I}} \int_{a_{ik}} \vec{\psi}_i \cdot (\vec{\mathbf{E}}|_{a_{ik}} \times \vec{n}_{ik}) = 0, \end{aligned} \right. \quad (33)$$

where $\vec{\phi}_i = \vec{\phi}|_{\tau_i}$ and $\vec{\psi}_i = \vec{\psi}|_{\tau_i}$. Summing up the identities in (33) with respect to i , we consider the following semi-discrete discontinuous Galerkin problem : find $(\vec{\mathbf{E}}_h(\cdot, t), \vec{\mathbf{H}}_h(\cdot, t)) \in V_p(\Omega_h) \times V_p(\Omega_h)$ such that, $\forall \tau_i \in \Omega_h$ and $\forall \vec{\phi}_h, \vec{\psi}_h \in V_p(\Omega_h)$,

$$\left\{ \begin{aligned} \sum_i \int_{\tau_i} \vec{\phi}_{hi} \cdot \bar{\epsilon}_i \partial_t \vec{\mathbf{E}}_i - \sum_i \int_{\tau_i} \vec{\mathbf{H}}_i \cdot \text{curl} \vec{\phi}_{hi} &+ \sum_{a_{ik} \in \mathcal{F}_h} \int_{a_{ik}} \llbracket \vec{\phi}_h \rrbracket_{ik}^i \cdot \{\vec{\mathbf{H}}_h\}_{ik} = 0, \\ \sum_i \int_{\tau_i} \vec{\psi}_{hi} \cdot \bar{\mu}_i \partial_t \vec{\mathbf{H}}_i + \sum_i \int_{\tau_i} \vec{\mathbf{E}}_i \cdot \text{curl} \vec{\psi}_{hi} &- \sum_{a_{ik} \in \mathcal{F}_h} \int_{a_{ik}} \llbracket \vec{\psi}_h \rrbracket_{ik}^i \cdot \{\vec{\mathbf{E}}_h\}_{ik} = 0, \\ \vec{\mathbf{E}}_h(0) = \Pi_h^p \vec{\mathbf{E}}_0 \quad \text{and} \quad \vec{\mathbf{H}}_h(0) &= \Pi_h^p \vec{\mathbf{H}}_0. \end{aligned} \right. \quad (34)$$

Here $\Pi_h^p : \mathbf{L}^2(\Omega) \rightarrow V_p(\Omega_h)$ is the \mathbf{L}^2 -projection onto $V_p(\Omega_h)$. The problem (34) can be rewritten in the following form: find $\vec{\mathbf{U}}_h = (\vec{\mathbf{E}}_h, \vec{\mathbf{H}}_h) \in V_p(\Omega_h) \times V_p(\Omega_h)$ such that:

$$J(\partial_t \vec{\mathbf{U}}_h, \vec{\mathbf{U}}_h) + a(\vec{\mathbf{U}}_h, \vec{\mathbf{U}}_h) + b(\vec{\mathbf{U}}_h, \vec{\mathbf{U}}_h) = 0, \quad \forall \vec{\mathbf{U}}_h = (\vec{\phi}_h, \vec{\psi}_h) \in V_p(\Omega_h) \times V_p(\Omega_h). \quad (35)$$

For $\vec{\mathbf{W}} = (\vec{u}, \vec{v})$ and $\vec{\mathbf{W}}' = (\vec{u}', \vec{v}')$, the bilinear forms J, a and b defined on $V_p(\Omega_h) \times V_p(\Omega_h)$ are given by:

$$\left\{ \begin{aligned} J(\vec{\mathbf{W}}, \vec{\mathbf{W}}') &= \sum_i \int_{\tau_i} (\bar{\epsilon} \vec{u} \cdot \vec{u}' + \bar{\mu} \vec{v} \cdot \vec{v}'), \\ a(\vec{\mathbf{W}}, \vec{\mathbf{W}}') &= \sum_i \int_{\tau_i} (\vec{u} \cdot \text{curl} \vec{v}' - \vec{v} \cdot \text{curl} \vec{u}'), \\ b(\vec{\mathbf{W}}, \vec{\mathbf{W}}') &= \sum_{a_{ik} \in \mathcal{F}_h} \int_{a_{ik}} (\{\vec{v}\} \cdot \llbracket \vec{u}' \rrbracket - \{\vec{u}\} \cdot \llbracket \vec{v}' \rrbracket), \end{aligned} \right. \quad (36)$$

taking into account that, for boundary faces $a_{ik} \in \mathcal{F}_h^B$ we have $\{\vec{v}\} = \vec{v}$. The semi-discrete discontinuous Galerkin formulation (35) is consistent with the original continuous problem (27) in the following sense: if $\vec{\mathbf{U}} = (\vec{\mathbf{E}}, \vec{\mathbf{H}})$ is the exact solution of (27), such that $\forall h, \forall t \in [0, T]$, $(\vec{\mathbf{E}}(\cdot, t), \vec{\mathbf{H}}(\cdot, t)) \in \mathbf{H}^s(\Omega) \times \mathbf{H}^s(\Omega)$, then we have:

$$J(\partial_t \vec{\mathbf{U}}, \vec{\mathbf{U}}') + a(\vec{\mathbf{U}}, \vec{\mathbf{U}}') + b(\vec{\mathbf{U}}, \vec{\mathbf{U}}') = 0, \quad \forall \vec{\mathbf{U}}' \in V_p(\Omega_h) \times V_p(\Omega_h). \quad (37)$$

The following approximation results will be used to bound the error [1]-[21]

Lemma 3.4 (Babuska and Suri [1]) Let $\tau_i \in \Omega_h$ and suppose that $\vec{u} \in \mathbf{H}^{s+1}(\tau_i)$ for $s \geq 0$. Let Π be a linear continuous operator from $\mathbf{H}^{s+1}(\tau_i)$ onto $\mathbb{P}_{p_i}(\tau_i)$, $p_i \geq 1$, such that $\Pi(\vec{u}) = \vec{u}$, $\forall \vec{u} \in \mathbb{P}_{p_i}(\tau_i)$. Then we have:

$$\|\vec{u} - \Pi(\vec{u})\|_{0,\tau_i} \leq C \frac{h_i^{\nu_i+1}}{p_i^{s+1}} \|\vec{u}\|_{s+1,\tau_i}, \quad (38)$$

$$\|\vec{u} - \Pi(\vec{u})\|_{0,\partial\tau_i} \leq C \frac{h_i^{\nu_i+\frac{1}{2}}}{p_i^{s+\frac{1}{2}}} \|\vec{u}\|_{s+1,\tau_i}, \quad (39)$$

where $\nu_i = \min\{s, p_i\}$ and C is a positive constant independent of u , h_i and p_i , but dependent on s and on the shape regularity of the mesh parameter η .

Lemma 3.5 (Schwab [21]) For all $q \in \mathbb{P}_{p_i}(\tau_i)$, $p_i \geq 1$, we have:

$$\|q\|_{0,\partial\tau_i}^2 \leq C_{inv} \frac{p_i^2}{h_i} \|q\|_{0,\tau_i}^2,$$

where C_{inv} is a positive constant depending only on the shape regularity of the mesh parameter η .

Let $\vec{\mathbf{U}} = (\vec{\mathbf{E}}, \vec{\mathbf{H}})$ and $\vec{\mathbf{U}}_h = (\vec{\mathbf{E}}_h, \vec{\mathbf{H}}_h)$. We denote by $\varepsilon_{\tau_i}(t)$ the local error and by $\varepsilon(t) = \sum_{\tau_i \in \Omega_j} \varepsilon_{\tau_i}(t)$ the global error. Then we have:

$$\begin{aligned} \varepsilon_{\tau_i}(t) &= \|\vec{\mathbf{E}} - \Pi_h^p \vec{\mathbf{E}} + \Pi_h^p \vec{\mathbf{E}} - \vec{\mathbf{E}}_h\|_{0,\tau_i}^2 + \|\vec{\mathbf{H}} - \Pi_h^p \vec{\mathbf{H}} + \Pi_h^p \vec{\mathbf{H}} - \vec{\mathbf{H}}_h\|_{0,\tau_i}^2 \\ &\leq 2(\|\vec{\mathbf{E}} - \Pi_h^p \vec{\mathbf{E}}\|_{0,\tau_i}^2 + \|\vec{\mathbf{H}} - \Pi_h^p \vec{\mathbf{H}}\|_{0,\tau_i}^2) + 2(\|\Pi_h^p \vec{\mathbf{E}} - \vec{\mathbf{E}}_h\|_{0,\tau_i}^2 + \|\Pi_h^p \vec{\mathbf{H}} - \vec{\mathbf{H}}_h\|_{0,\tau_i}^2) \\ &= 2\|\vec{\mathbf{U}} - \Pi_h^p \vec{\mathbf{U}}\|_{0,\tau_i}^2 + 2\|\Pi_h^p \vec{\mathbf{U}} - \vec{\mathbf{U}}_h\|_{0,\tau_i}^2 \\ &= 2\varepsilon_{\tau_i}^a + 2\varepsilon_{\tau_i}^b, \end{aligned}$$

where $\varepsilon_{\tau_i}^a$ is due to the error introduced by the polynomial approximation of the exact solution while $\varepsilon_{\tau_i}^b$ measures the errors associated with the semi-discrete approximation of Maxwell's equations.

To bound $\varepsilon_{\tau_i}^a$ we need only recall Lemma 3.4 to state

Lemma 3.6 Assume that $\vec{\mathbf{U}} \in \mathbf{H}^{s+1}(\tau_i) \times \mathbf{H}^{s+1}(\tau_i)$. Then there exists a constant C , dependent on s and on the shape regularity of the mesh η , but independent of $\vec{\mathbf{U}}$, h_i and p_i , such that:

$$\|\vec{\mathbf{U}} - \Pi_h^p \vec{\mathbf{U}}\|_{0,\tau_i} \leq C \frac{h_i^{\nu_i+1}}{p_i^{s+1}} \|\vec{\mathbf{U}}\|_{s+1,\tau_i}, \quad (40)$$

where $\nu_i = \min\{s, p_i\}$ and $s \geq 0$.

Theorem 3.1 Assume that a solution $(\vec{\mathbf{E}}(t), \vec{\mathbf{H}}(t)) \in \mathbf{H}^{s+1}(\tau_i) \times \mathbf{H}^{s+1}(\tau_i)$ with $s \geq 1/2$ to Maxwell's equations in $\Omega_h = \bigcup_i \tau_i$ exists. Then the numerical solution, $(\vec{\mathbf{E}}_h(t), \vec{\mathbf{H}}_h(t)) \in V_p(\Omega_h) \times V_p(\Omega_h)$, to the semi-discrete approximation (34) converges to the exact solution and the global error is bounded as:

$$\left(\|\vec{\mathbf{E}} - \vec{\mathbf{E}}_h\|_{0,\Omega}^2 + \|\vec{\mathbf{H}} - \vec{\mathbf{H}}_h\|_{0,\Omega}^2 \right)^{\frac{1}{2}} \leq C \left(\frac{h^{\nu+1}}{p_{\min}^{s+1}} + T \frac{h^\nu}{p_{\min}^{s-\frac{1}{2}}} \right) \max_{t \in [0, T]} \|(\vec{\mathbf{E}}(t), \vec{\mathbf{H}}(t))\|_{s+1,\Omega}, \quad (41)$$

where $\nu = \min\{s, p_{\min}\}$ and $p_{\min} = \min\{p_i, \tau_i \in \Omega_h\}$, $p_i \geq 1$. The constant $C > 0$ depends on the material properties and on the shape regularity of the mesh parameter η , but not on p_{\min} and h .

Proof. Let $\vec{\mathbf{q}} = \vec{\mathbf{U}} - \vec{\mathbf{U}}_h$. Since $\Pi_h^p \vec{\mathbf{U}}_h = \vec{\mathbf{U}}_h$, we have $\sum_i \varepsilon_{\tau_i}^b = \|\Pi_h^p \vec{\mathbf{q}}\|_{0,\Omega}^2$. To obtain a bound for $\|\Pi_h^p \vec{\mathbf{q}}\|_{0,\Omega}$, we introduce $\sigma(t) = \frac{1}{2} J(\Pi_h^p \vec{\mathbf{q}}(t), \Pi_h^p \vec{\mathbf{q}}(t))$ with $\Pi_h^p \vec{\mathbf{q}}(\cdot, t)$ belongs to $V_p(\Omega_h) \times V_p(\Omega_h)$. Using the discrete initial conditions of (34), we have $\sigma(0) = 0$ and then, for $0 < t \leq T$,

$$\sigma(t) = \frac{1}{2} \int_0^t \frac{d}{ds} J(\Pi_h^p \vec{\mathbf{q}}(s), \Pi_h^p \vec{\mathbf{q}}(s)) ds = \int_0^t J(\partial_s \Pi_h^p \vec{\mathbf{q}}(s), \Pi_h^p \vec{\mathbf{q}}(s)) ds.$$

For any $\vec{\mathbf{U}}_h \in V_p(\Omega_h) \times V_p(\Omega_h)$, we have $a(\vec{\mathbf{U}}_h, \vec{\mathbf{U}}_h) + b(\vec{\mathbf{U}}_h, \vec{\mathbf{U}}_h) = 0$, and we get:

$$\sigma(t) = \int_0^t (J(\partial_s \Pi_h^p \vec{\mathbf{q}}(s), \Pi_h^p \vec{\mathbf{q}}(s)) + a(\Pi_h^p \vec{\mathbf{q}}(s), \Pi_h^p \vec{\mathbf{q}}(s)) + b(\Pi_h^p \vec{\mathbf{q}}(s), \Pi_h^p \vec{\mathbf{q}}(s))) ds. \quad (42)$$

Subtracting (35) from the consistency result (37) with $\vec{\mathbf{U}}' = \vec{\mathbf{U}}'_h = \Pi_h^p \vec{\mathbf{q}}(s)$ yields:

$$J(\partial_s \vec{\mathbf{q}}(s), \Pi_h^p \vec{\mathbf{q}}(s)) + a(\vec{\mathbf{q}}(s), \Pi_h^p \vec{\mathbf{q}}(s)) + b(\vec{\mathbf{q}}(s), \Pi_h^p \vec{\mathbf{q}}(s)) = 0. \quad (43)$$

Now, subtracting the above equality (43) from (42) leads to:

$$\begin{aligned} \sigma(t) = \int_0^t & \left(J([\Pi_h^p \partial_s \vec{\mathbf{U}} - \partial_s \vec{\mathbf{U}}](s), \Pi_h^p \vec{\mathbf{q}}(s)) + a([\Pi_h^p \vec{\mathbf{U}} - \vec{\mathbf{U}}](s), \Pi_h^p \vec{\mathbf{q}}(s)) \right. \\ & \left. + b([\Pi_h^p \vec{\mathbf{U}} - \vec{\mathbf{U}}](s), \Pi_h^p \vec{\mathbf{q}}(s)) \right) ds. \end{aligned}$$

Since Π_h^p is a projector onto $V_p(\Omega_h)$ and $\Pi_h^p \vec{\mathbf{q}}(\cdot, t)$ belongs to $V_p(\Omega_h) \times V_p(\Omega_h)$, then $J(\Pi_h^p \partial_s \vec{\mathbf{U}} - \partial_s \vec{\mathbf{U}}, \Pi_h^p \vec{\mathbf{q}}) = 0$ and $a(\Pi_h^p \vec{\mathbf{U}} - \vec{\mathbf{U}}, \Pi_h^p \vec{\mathbf{q}}) = 0$. Using the lower bound $C_1 > 0$ of $\bar{\varepsilon}$ and $\bar{\mu}$ (28), we thus get:

$$\frac{C_1}{2} \|\Pi_h^p \vec{\mathbf{q}}(t)\|_{0,\Omega}^2 \leq \int_0^t b([\Pi_h^p \vec{\mathbf{U}} - \vec{\mathbf{U}}](s), \Pi_h^p \vec{\mathbf{q}}(s)) ds. \quad (44)$$

Now, we bound the surface integrals deriving from the definition of $b(\cdot, \cdot)$. We assume that $\vec{\mathbf{q}} = (\vec{\mathbf{q}}^E, \vec{\mathbf{q}}^H)$, where $\vec{\mathbf{q}}^E$ and $\vec{\mathbf{q}}^H$ denote the error in $\vec{\mathbf{E}}$ and $\vec{\mathbf{H}}$ respectively. Let $a_{ik} \in \mathcal{F}_h^I$ be an internal interface shared by the tetrahedra τ_i and τ_k . We denote by $\mathbb{I}^E = \int_{a_{ik}} \{\Pi_h^p \vec{\mathbf{H}} - \vec{\mathbf{H}}\}_{ik} \cdot [\Pi_h^p \vec{\mathbf{q}}^E]_{ik}$, we have, using the Cauchy-Schwarz-Buniakovsky (CSB) inequality:

$$\begin{aligned} \mathbb{I}^E & \leq \frac{1}{2} \left(\int_{a_{ik}} [(\Pi_h^p \vec{\mathbf{H}}_i - \vec{\mathbf{H}}_i) + (\Pi_h^p \vec{\mathbf{H}}_k - \vec{\mathbf{H}}_k)]^2 \right)^{\frac{1}{2}} \left(\int_{a_{ik}} \vec{n}_{ik} (\Pi_h^p \vec{\mathbf{q}}^E)_i|_{a_{ik}} + \vec{n}_{ki} (\Pi_h^p \vec{\mathbf{q}}^E)_k|_{a_{ik}} \right)^{\frac{1}{2}} \\ & \leq \left(\|\Pi_h^p \vec{\mathbf{H}}_i - \vec{\mathbf{H}}_i\|_{0,a_{ik}}^2 + \|\Pi_h^p \vec{\mathbf{H}}_k - \vec{\mathbf{H}}_k\|_{0,a_{ik}}^2 \right)^{\frac{1}{2}} \left(\|(\Pi_h^p \vec{\mathbf{q}}^E)_i\|_{0,a_{ik}}^2 + \|(\Pi_h^p \vec{\mathbf{q}}^E)_k\|_{0,a_{ik}}^2 \right)^{\frac{1}{2}}. \end{aligned}$$

Using Lemma 3.4 and Lemma 3.5, yields:

$$\mathbb{I}^E \leq \left(C \frac{h_i^{\nu_i + \frac{1}{2}}}{p_i^{s + \frac{1}{2}}} \|\vec{\mathbf{H}}\|_{s+1,\tau_i} + C \frac{h_k^{\nu_k + \frac{1}{2}}}{p_k^{s + \frac{1}{2}}} \|\vec{\mathbf{H}}\|_{s+1,\tau_k} \right)^{\frac{1}{2}} \left(C \frac{p_i^2}{h_i} \|\Pi_h^p \vec{\mathbf{q}}^E\|_{0,\tau_i}^2 + C \frac{p_k^2}{h_k} \|\Pi_h^p \vec{\mathbf{q}}^E\|_{0,\tau_k}^2 \right)^{\frac{1}{2}}.$$

According to the assumptions (2), we finally get:

$$\mathbb{I}^E \leq K(\kappa_1, \kappa_2) \frac{h_i^\nu}{p_i^{s - \frac{1}{2}}} \left(\|\vec{\mathbf{H}}\|_{s+1,\tau_i}^2 + \|\vec{\mathbf{H}}\|_{s+1,\tau_k}^2 \right)^{\frac{1}{2}} \left(\|\Pi_h^p \vec{\mathbf{q}}^E\|_{0,\tau_i}^2 + \|\Pi_h^p \vec{\mathbf{q}}^E\|_{0,\tau_k}^2 \right)^{\frac{1}{2}}, \quad (45)$$

where $K > 0$ does not depend on h_i and p_i , but depends on κ_1 and κ_2 , and on the local material properties $(\bar{\epsilon}_{i/k}, \bar{\mu}_{i/k})$ associated to τ_i and τ_k .

The term $\mathbb{I}^H = \int_{a_{ik}} \{\Pi_h^p \vec{\mathbf{E}} - \vec{\mathbf{E}}\}_{ik} \cdot \llbracket \Pi_h^p \vec{\mathbf{q}}^H \rrbracket_{ik}$ is treated in the same way, yielding the result:

$$\mathbb{I}^H \leq K(\kappa_1, \kappa_2) \frac{h_i^\nu}{p_i^{s-\frac{1}{2}}} (\|\vec{\mathbf{E}}\|_{s+1, \tau_i}^2 + \|\vec{\mathbf{E}}\|_{s+1, \tau_k}^2)^{\frac{1}{2}} (\|\Pi_h^p \vec{\mathbf{q}}^H\|_{0, \tau_i}^2 + \|\Pi_h^p \vec{\mathbf{q}}^H\|_{0, \tau_k}^2)^{\frac{1}{2}}. \quad (46)$$

For boundary interfaces $a_{ik} \in \mathcal{F}_h^B$, we obtain the same upper bounds as (45) and (46) but without the norms on τ_k .

Summing up with respect to all $\tau_i \in \Omega_h$, and using the CSB inequality, yields:

$$b(\llbracket \Pi_h^p \vec{\mathbf{U}} - \vec{\mathbf{U}} \rrbracket(s), \Pi_h^p \vec{\mathbf{q}}(s)) \leq K(\kappa_1, \kappa_2) \frac{h^\nu}{p_{\min}^{s-\frac{1}{2}}} \|\Pi_h^p \vec{\mathbf{q}}(s)\|_{0, \Omega} \|(\vec{\mathbf{E}}(s), \vec{\mathbf{H}}(s))\|_{s+1, \Omega}. \quad (47)$$

Integrating in $t \in [0, T]$ and combining this with Lemma 3.6 establishes the result and proves convergence on weak assumptions of local, elementwise smoothness of the solution. \square

Corollary 3.1 *Under the assumptions of Theorem 3.1 and assuming that $(\vec{\mathbf{E}}(t), \vec{\mathbf{H}}(t)) \in \mathbf{H}^s(\tau_i) \times \mathbf{H}^s(\tau_i)$, $s \geq 3/2$, the global error is bounded as:*

$$\left(\|\vec{\mathbf{E}} - \vec{\mathbf{E}}_h\|_{0, \Omega}^2 + \|\vec{\mathbf{H}} - \vec{\mathbf{H}}_h\|_{0, \Omega}^2 \right)^{\frac{1}{2}} \leq C \left(\frac{h^\nu}{p_{\min}^s} + T \frac{h^{\nu-1}}{p_{\min}^{s-\frac{3}{2}}} \right) \max_{t \in [0, T]} \|(\vec{\mathbf{E}}(t), \vec{\mathbf{H}}(t))\|_{s, \Omega}, \quad (48)$$

where $\nu = \min\{s, p_{\min} + 1\}$ and $p_{\min} = \min\{p_i, \tau_i \in \Omega_h\}$, $p_i \geq 1$. The constant $C > 0$ depends on the material properties and on the shape regularity of the mesh η , but not on p_{\min} and h .

We have hence established the semi-discrete result that the error cannot grow faster than linearly in time and that we can control the growth rate by adapting the resolution parameters h and p accordingly. As we shall verify in Sec. 4 this linear growth is a sharp result. However, the numerical experiments will also show that we can expect that the growth rate approaches zero spectrally fast when increasing the approximation order p provided that the solution is sufficiently smooth.

Note that the convergence result of Corollary 3.1 is different from the one obtained by Fezoui *et al* [14]. The convergence result in [14] considers only the case of a conforming discontinuous Galerkin formulation where the interpolation degree is constant. The result presented here remains valid on any kind of mesh and discontinuous elements, including hp -type or non-conformal refinement.

Now, we give the consistency order of the time-discretized problem. The discretized scheme (6) can be formally seen as the discretization in time of a system of ODEs (20). The estimation of the consistency error comes directly from Taylor expansions. If $(\vec{\mathbf{E}}_h^{n+1}, \vec{\mathbf{H}}_h^{n+\frac{3}{2}})$ is computed from $\vec{\mathbf{E}}_h^n = \vec{\mathbf{E}}_h(t^n)$ and $\vec{\mathbf{H}}_h^{n+\frac{1}{2}} = \vec{\mathbf{H}}_h(t^{n+\frac{1}{2}})$ by (6) where $(\vec{\mathbf{E}}_h(\cdot), \vec{\mathbf{H}}_h(\cdot))$ denotes the semi-discrete solution of (34), then there exists a constant C independent of Δt and h , but dependent on the order of the leap-frog scheme N , such that:

$$\begin{aligned} & \|\vec{\mathbf{E}}_h^{n+1} - \vec{\mathbf{E}}_h^n\|_{0, \tau_i} + \|\vec{\mathbf{H}}_h^{n+\frac{3}{2}} - \vec{\mathbf{H}}_h^{n+\frac{1}{2}}\|_{0, \tau_i} \leq \\ & C \Delta t^{N+1} \left(\sum_{m=1}^{N/2+1} (\|\partial_t^m \vec{\mathbf{E}}_h\|_{0, \tau_i}^2)^{\frac{1}{2}} + \sum_{m=1}^{N/2+1} (\|\partial_t^m \vec{\mathbf{H}}_h\|_{0, \tau_i}^2)^{\frac{1}{2}} \right). \end{aligned} \quad (49)$$

Provided that the exact solution of the Maxwell system (27) is regular enough, $(\partial_t^m \vec{\mathbf{E}}_h, \partial_t^m \vec{\mathbf{H}}_h)$ are some discrete approximation of $(\partial_t^m \vec{\mathbf{E}}, \partial_t^m \vec{\mathbf{H}})$ which is also a solution of Maxwell equations and, $\|\partial_t^m \vec{\mathbf{E}}_h\|_{0, \tau_i}$ and $\|\partial_t^m \vec{\mathbf{H}}_h\|_{0, \tau_i}$ can be bounded independently from h , which proves that the consistency error is of order $\mathcal{O}(\Delta t^N)$.

3.3 Convergence of the divergence error

In the absence of sources, it is well known that the electric and the magnetic fields must remain solenoidal¹ throughout the computation. Indeed, taking the divergence of Eqs. (27a) and applying Eqs. (27c) in combination with Gauss' law for charge conservation immediately confirms that if the initial conditions satisfy Eqs. (27c), and the fields are evolved according to Maxwell's equations Eqs. (27a), the solution will satisfy Eqs. (27c) at all times. Hence, one can view Eqs. (27c) as a consistency condition on the initial conditions and limit the solution to the time-dependent part of Maxwell's equations, Eqs. (27a). The scheme in Eqs. (6) does not solve Eqs. (1), however, but rather an approximation to it. Hence one needs to consider the question of how well Eqs. (6) conserve the divergence.

Using the results of Sec. 3.2 we can state the following result.

Theorem 3.2 *Assume that a solution $\vec{\mathbf{U}} = (\vec{\mathbf{E}}(t), \vec{\mathbf{H}}(t)) \in \mathbf{H}^s(\tau_i) \times \mathbf{H}^s(\tau_i)$ with $s \geq 7/2$ to Maxwell's equations in $\Omega_h = \bigcup_i \tau_i$ exists. Then there exist a constant C dependent on s and the shape regularity of the mesh parameter η , but independent of $\vec{\mathbf{U}}$, h , and p , such that the divergence of the numerical solution $\vec{\mathbf{U}}_h$ to the semi-discrete approximation (34) is bounded as:*

$$\left(\|\nabla \cdot (\vec{\mathbf{E}} - \vec{\mathbf{E}}_h)\|_{0,\Omega}^2 + \|\nabla \cdot (\vec{\mathbf{H}} - \vec{\mathbf{H}}_h)\|_{0,\Omega}^2 \right)^{\frac{1}{2}} \leq C \left(\frac{h^{\nu-1}}{p_{\min}^{s-1}} + T \frac{h^{\nu-2}}{p_{\min}^{s-\frac{7}{2}}} \right) \max_{t \in [0, T]} \|(\vec{\mathbf{E}}(t), \vec{\mathbf{H}}(t))\|_{s,\Omega}, \quad (50)$$

where $\nu = \min\{s, p_{\min} + 1\}$ and $p_{\min} = \min\{p_i, \tau_i \in \Omega_h\}$, $p_i \geq 1$.

Proof. Consider the local divergence of $\vec{\mathbf{H}}$ on any $\tau_i \in \Omega_h$ we have:

$$\|\nabla \cdot (\vec{\mathbf{H}} - \vec{\mathbf{H}}_h)\|_{0,\tau_i}^2 \leq 2\|\nabla \cdot (\vec{\mathbf{H}} - \Pi_h^p \vec{\mathbf{H}})\|_{0,\tau_i}^2 + 2\|\nabla \cdot (\Pi_h^p \vec{\mathbf{H}} - \vec{\mathbf{H}}_h)\|_{0,\tau_i}^2. \quad (51)$$

The first term can be bounded using Lemma 3.4 as:

$$\|\nabla \cdot (\vec{\mathbf{H}} - \Pi_h^p \vec{\mathbf{H}})\|_{0,\tau_i} \leq C \frac{h_i^{\nu_i-1}}{p_i^{s-1}} \|\vec{\mathbf{H}}\|_{s,\tau_i}, \quad (52)$$

where $\nu_i = \min\{s, p_i + 1\}$ and $s \geq 1$.

Using the inverse inequality [21]:

$$\|\nabla \cdot \vec{\mathbf{u}}_h\|_{0,\tau_i} \leq C \frac{p_i^2}{h_i} \|\vec{\mathbf{u}}_h\|_{s,\tau_i}, \quad (53)$$

for all $\vec{\mathbf{u}}_h \in \mathbb{P}_{p_i}(\tau_i)$, we can bound the second term as:

$$\begin{aligned} \|\nabla \cdot (\Pi_h^p \vec{\mathbf{H}} - \vec{\mathbf{H}}_h)\|_{0,\tau_i} &\leq C \frac{p_i^2}{h_i} \|\Pi_h^p \vec{\mathbf{H}} - \vec{\mathbf{H}}_h\|_{0,\tau_i} \\ &\leq CT \frac{p_i^2}{h_i} \frac{h_i^{\nu-1}}{p_i^{s-\frac{3}{2}}} \|(\vec{\mathbf{E}}, \vec{\mathbf{H}})\|_{s,\tau_i} \\ &\leq CT \frac{h_i^{\nu-2}}{p_i^{s-\frac{7}{2}}} \|(\vec{\mathbf{E}}, \vec{\mathbf{H}})\|_{s,\tau_i}, \end{aligned} \quad (54)$$

¹A solenoidal vector is a vector field \mathbf{v} with zero divergence, $\nabla \cdot \mathbf{v} = 0$.

by combining (44) with (47). An equivalent bound can be obtained for the divergence of $\vec{\mathbf{E}}_h$ in the case of a source free medium which, combined with the above, yields the result. \square

As could be expected, the result inherits the temporal linear growth from the convergence result and confirms the possibility of recovering spectral convergence of the divergence under the assumption of sufficient smoothness of the solutions. It should be noted that while the result confirms high-order accuracy and convergence, the estimate for the actual convergence rate is certainly suboptimal and leaves room for improvement.

4 Numerical validation

In the following, we shall discuss the validity of the main theoretical results of the previous sections through the numerical solution of the two-dimensional Maxwell's equations in the TM polarization, *i.e.* we solve for (H_x, H_y, E_z) .

We consider the propagation of an eigenmode which is a standing wave of frequency $f = 212$ MHz and wavelength $\lambda = 1.4$ m in a unitary metallic cavity with $\epsilon = \mu = 1$ in normalized units. Owing to the existence of an exact analytical solution, this problem allows us to appreciate the numerical results at any point and time in the cavity. Numerical simulations make use of a non-conforming locally refined triangular meshes of the square $[0, 1] \times [0, 1]$ as shown on Fig. 4. In the sequel, we compare the LF₂ and LF₄ schemes using the DGTD- \mathbb{P}_p and DGTD- $\mathbb{P}_{p_c}:\mathbb{P}_{p_f}$ methods previously studied in [8]-[9]-[11]. In Tab. 2, we summarize the CFL values of the LF₂ based DGTD- \mathbb{P}_p and DGTD- $\mathbb{P}_{p_c}:\mathbb{P}_{p_f}$ methods. The CFL values of the LF₄ schemes are given by $\text{CFL}(\text{LF}_4) = 2.847 \text{ CFL}(\text{LF}_2)$. If $p_c \neq p_f$, the DGTD- $\mathbb{P}_{p_c}:\mathbb{P}_{p_f}$ method has the same stability limit as the DGTD- $\mathbb{P}_{\min\{p_c, p_f\}}$ method, as long as the mesh is actually refined.

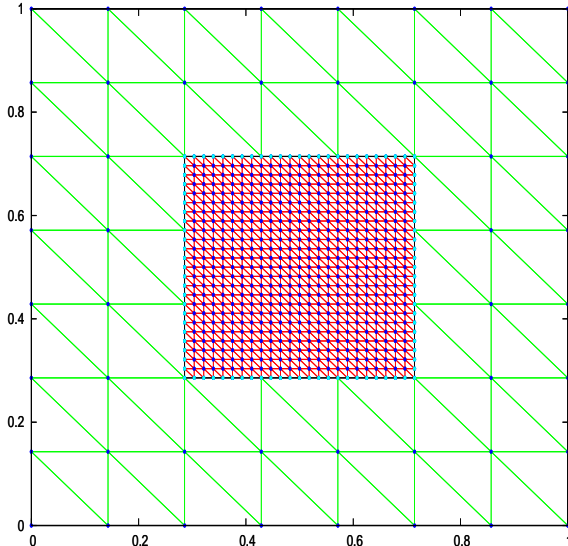


Figure 4: *Example of a non-conforming locally refined triangular mesh.*

As a first verification of the theoretical estimates, we consider a non-conforming mesh consists of 782 triangles and 442 nodes (36 of them are hanging nodes). All simulations are carried out for $t = 150$ which corresponds to 106 periods. We plot on Fig. 5 the time evolution of the L^2 error of the DGTD- \mathbb{P}_p and DGTD- $\mathbb{P}_{p_c}:\mathbb{P}_{p_f}$ methods using the LF₂ and LF₄ schemes. Tab. 3 gives the final L^2 error, the number of degrees of freedom and the CPU time to reach $t = 150$. It can be observed from Fig. 5 that the gain in the L^2 error is notable when the accuracy in space and time are increased. Moreover, it is clear from (17) and Lemma 3.2 that, for a given mesh, each time step of LF₄ scheme requires 2

times more memory than the LF_2 , but its stability limit is almost 2.85 times less restrictive. Then, the LF_4 schemes requires almost 1.5 times less CPU time and is roughly 15 times more accurate than the LF_2 scheme based on the observed L^2 errors. Furthermore, for a given accuracy, the LF_4 based $DGTD-\mathbb{P}_{p_c}:\mathbb{P}_{p_f}$ method requires less CPU time than the LF_4 based $DGTD-\mathbb{P}_p$ method.

Table 2: The CFL values of the LF_2 $DGTD-\mathbb{P}_p$ and $DGTD-\mathbb{P}_{p_c}:\mathbb{P}_{p_f}$ methods.

$p =$	1	2	3	4	5	6	7	8	9	10
CFL(LF_2)	0.3	0.2	0.1	0.08	0.06	0.045	0.035	0.03	0.025	0.02
$p_c:p_f =$	3:2	4:2	4:3	5:3	5:4	6:5	7:6	8:7	9:8	10:9
CFL(LF_2)	0.2	0.2	0.1	0.1	0.08	0.06	0.045	0.035	0.03	0.025

Fig. 6 illustrates the numerical h -convergence of the $DGTD-\mathbb{P}_p$ and $DGTD-\mathbb{P}_{p_c}:\mathbb{P}_{p_f}$ methods. Corresponding asymptotic convergence orders are summarized in Tab. 4. As it could be expected from the use of a N th accurate time integration scheme, the asymptotic convergence order is bounded by N independently of the approximation order p . On Fig. 7 we show the numerical p -convergence of the $DGTD-\mathbb{P}_p$ and $DGTD-\mathbb{P}_{p_c}:\mathbb{P}_{p_f}$ methods for different approximation orders p and different mesh resolutions h . Corresponding L^2 errors are given in Tab. 5 and 6. Following the main result, Theorem 3.1, we expect that the error grows at most linearly in time and that the growth rate should vanish spectrally for smooth solution. The results on Fig. 7 and in Tab. 5 and 6 not only confirm the validity of both statements but also illustrate that Theorem 3.1 is sharp, *i.e.* we cannot in general guarantee slower than linear growth, although we can control the growth rate by the approximation order p .

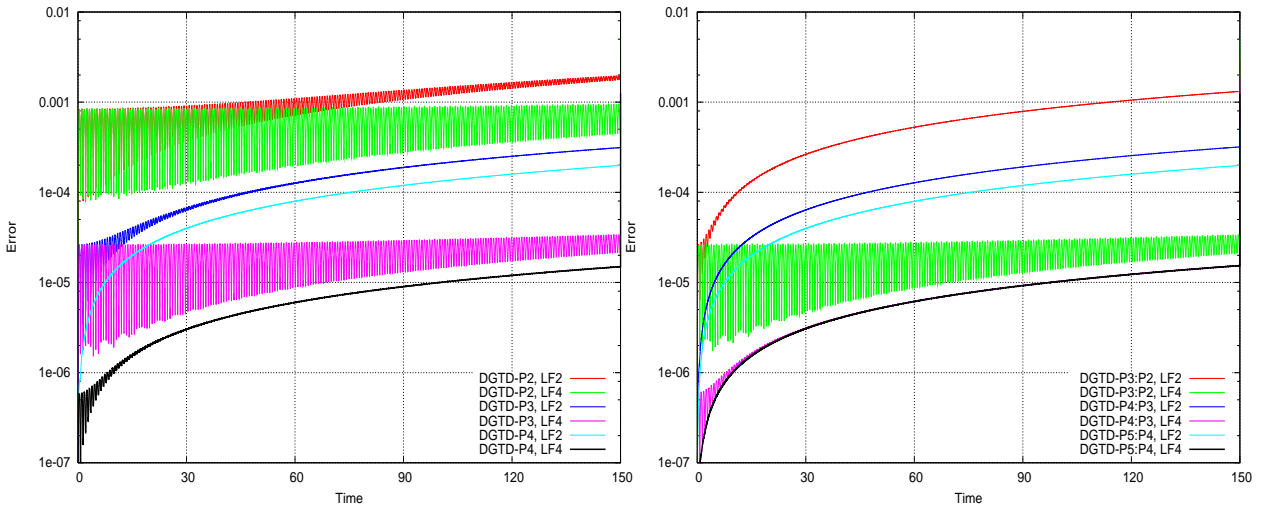


Figure 5: Time evolution of the L^2 error. $DGTD-\mathbb{P}_p$ (left) and $DGTD-\mathbb{P}_{p_c}:\mathbb{P}_{p_f}$ (right) methods.

We conclude this experimental study by considering the numerical behavior of the divergence error. For this purpose, we still consider the eigenmode problem. The computational domain is discretized by a non-conforming locally refined mesh with 48 triangles (32 of them in the refined region) and 37 nodes (16 of them are hanging nodes), which corresponds to a grid resolution of 5 points per wavelength. Simulations are carried out for $t = 30$ which corresponds to 20 periods. Fig. 8 shows the global L^2 error of the divergence of \vec{H} as a function of time and the approximation order p using respectively the $DGTD-\mathbb{P}_p$ and $DGTD-\mathbb{P}_{p_c}:\mathbb{P}_{p_f}$ methods. One can observe that for $p \leq N + 2$, the error vanishes faster than for $p > N + 2$, N being the order of the leap-frog (LF_N) scheme.

Table 3: # DOF, L^2 -error and CPU time using the LF_2 and LF_4 based DGTD methods.

DGTD- \mathbb{P}_p method		LF ₂		LF ₄	
p	# DOF	Error	CPU (min)	Error	CPU (min)
2	4692	1.8E-03	11	5.5E-04	8
3	7820	3.1E-04	39	2.4E-05	28
4	11730	1.9E-04	98	1.5E-05	70
5	16422	1.5E-04	220	1.3E-05	155

DGTD- $\mathbb{P}_{p_c}:\mathbb{P}_{p_f}$ method		LF ₂		LF ₄	
$p_c:p_f$	# DOF	Error	CPU (min)	Error	CPU (min)
3:2	6668	1.3E-03	17	2.3E-05	12
4:2	9138	1.3E-03	27	1.5E-05	19
4:3	10290	3.2E-04	61	1.5E-05	44
5:4	14694	2.0E-04	134	1.4E-05	95

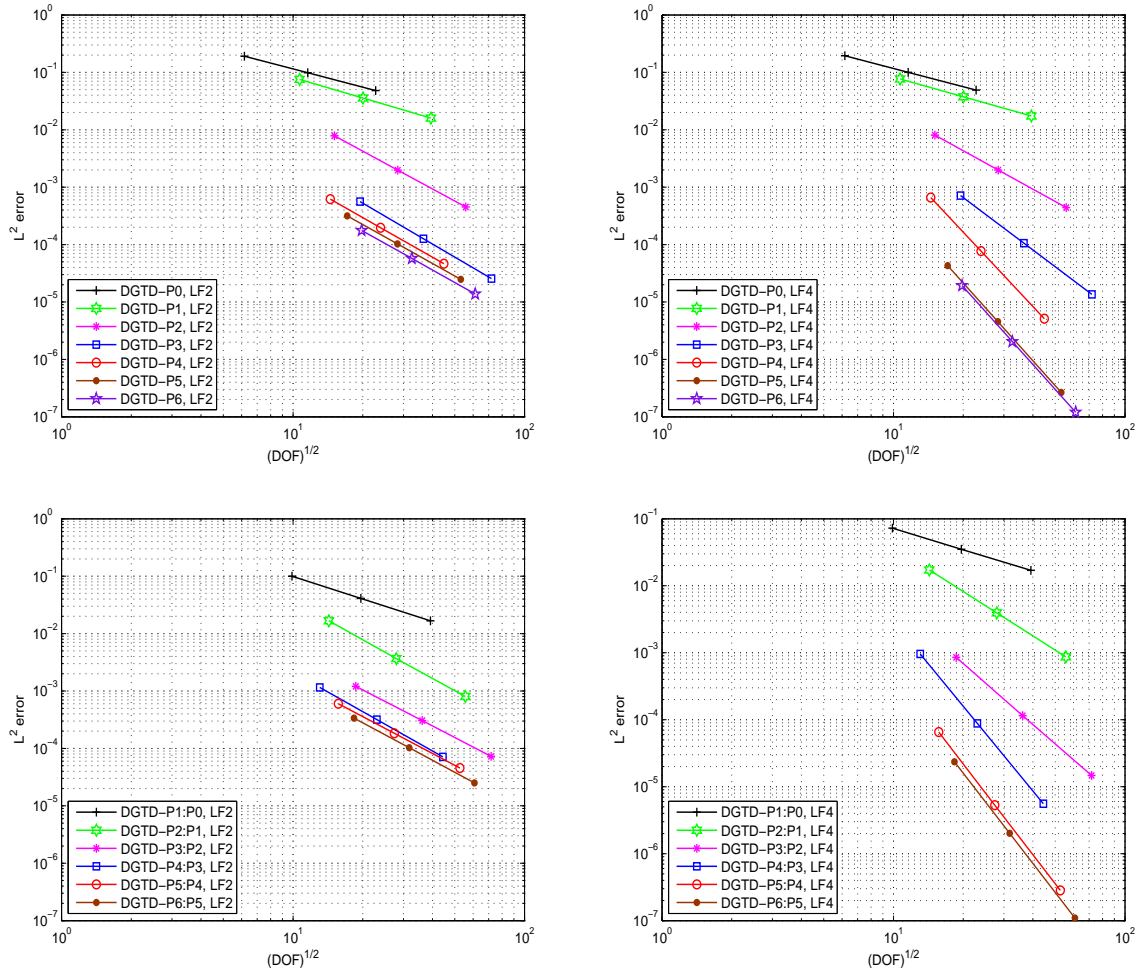

 Figure 6: h -convergence of the DGTD- \mathbb{P}_p (top) and DGTD- $\mathbb{P}_{p_c}:\mathbb{P}_{p_f}$ (bottom) methods. L^2 error as a function of the square root of #DOF.

Table 4: Asymptotic convergence orders of the LF_2 and LF_4 based DGTD methods.

DGTD- \mathbb{P}_p method, $p =$	0	1	2	3	4	5	6
LF_2 scheme	1.06	1.19	2.18	2.37	2.29	2.25	2.26
LF_4 scheme	1.06	1.14	2.23	3.03	4.30	4.50	4.50
DGTD- $\mathbb{P}_{p_c}:\mathbb{P}_{p_f}$ method, $p_c:p_f =$	1:0	2:1	3:2	4:3	5:4	6:5	
LF_2 scheme	1.30	2.23	2.08	2.27	2.13	2.17	
LF_4 scheme	1.05	2.20	3.01	4.21	4.50	4.48	

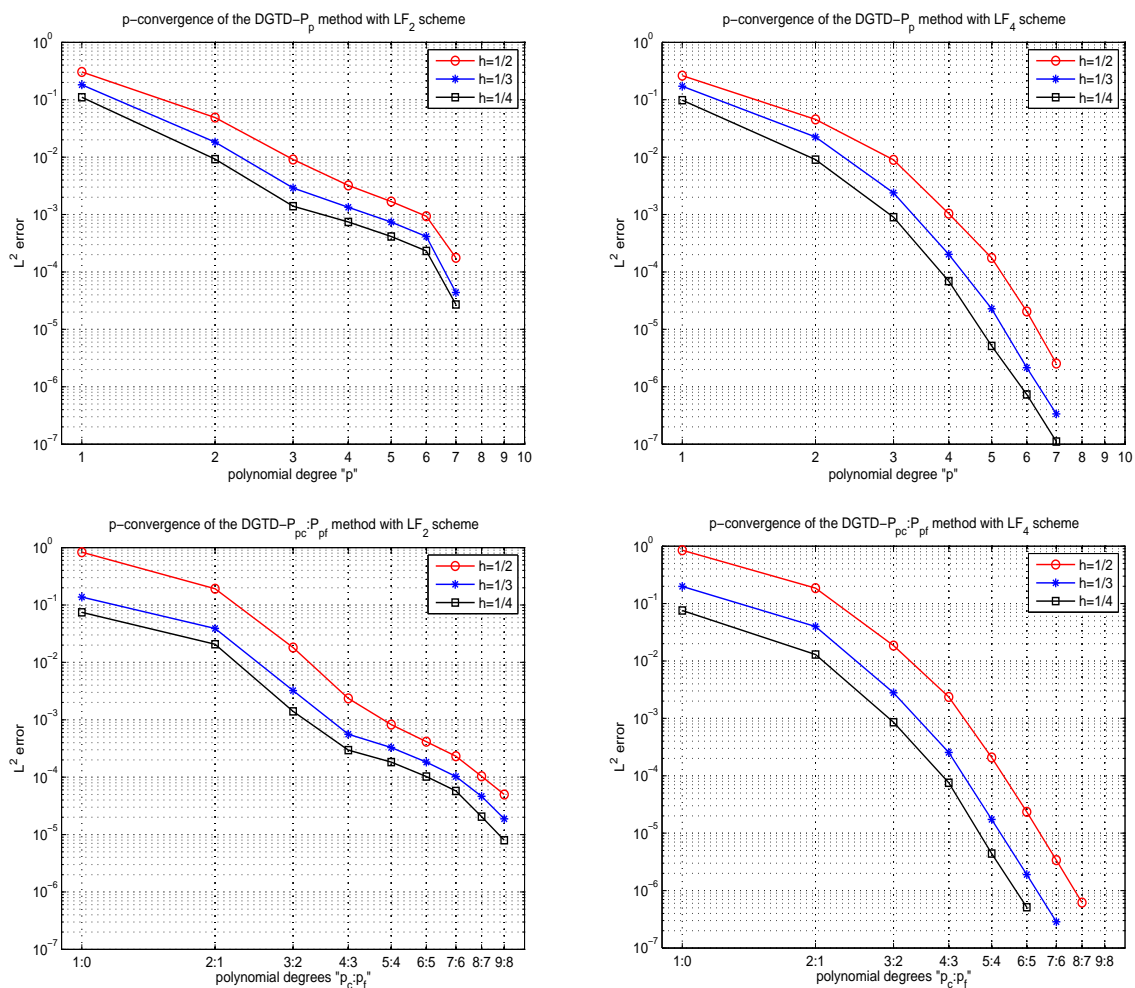
Figure 7: p -convergence of the DGTD- \mathbb{P}_p (top) and DGTD- $\mathbb{P}_{p_c}:\mathbb{P}_{p_f}$ (bottom) methods. L^2 error as a function of the approximation order p .

Table 5: p -convergence of the DGTD- \mathbb{P}_p method.

DGTD- \mathbb{P}_p method						
p	$h = 1/2$		$h = 1/3$		$h = 1/4$	
	LF ₂	LF ₄	LF ₂	LF ₄	LF ₂	LF ₄
1	3.0E-01	2.6E-01	1.8E-01	1.7E-01	1.1E-01	9.8E-02
2	4.9E-02	4.5E-02	1.8E-02	2.2E-02	9.2E-03	9.0E-03
3	9.1E-03	8.9E-03	2.8E-03	2.4E-03	1.4E-03	8.9E-04
4	3.2E-02	1.0E-03	1.3E-03	2.0E-04	7.4E-04	6.9E-05
5	1.6E-02	1.7E-04	7.4E-04	2.2E-05	4.1E-04	5.1E-06
6	9.3E-04	2.0E-05	4.1E-04	2.1E-06	2.3E-04	7.3E-07
7	1.7E-04	2.5E-06	4.4E-05	3.3E-07	2.7E-05	1.1E-07

Table 6: p -convergence of the DGTD- $\mathbb{P}_{p_c}:\mathbb{P}_{p_f}$ method.

DGTD- \mathbb{P}_p method						
$p_c:p_f$	$h = 1/2$		$h = 1/3$		$h = 1/4$	
	LF ₂	LF ₄	LF ₂	LF ₄	LF ₂	LF ₄
1:0	8.3E-01	8.5E-01	1.3E-01	1.9E-01	7.4E-02	7.6E-02
2:1	1.9E-01	1.8E-01	3.9E-02	3.9E-02	2.1E-02	1.3E-02
3:2	1.8E-02	1.8E-02	3.2E-03	2.7E-03	1.4E-03	8.5E-04
4:3	2.3E-03	2.3E-03	5.6E-04	2.5E-04	2.9E-04	7.6E-05
5:4	8.2E-04	2.0E-04	3.2E-04	1.7E-05	1.8E-04	4.4E-06
6:5	4.1E-04	2.3E-05	1.8E-04	1.9E-06	1.0E-04	4.7E-07
7:6	2.3E-04	3.4E-06	1.0E-04	2.8E-07	5.7E-05	-
8:7	1.0E-04	6.1E-07	4.6E-05	-	2.1E-05	-
9:8	4.9E-05	-	1.9E-05	-	7.9E-06	-

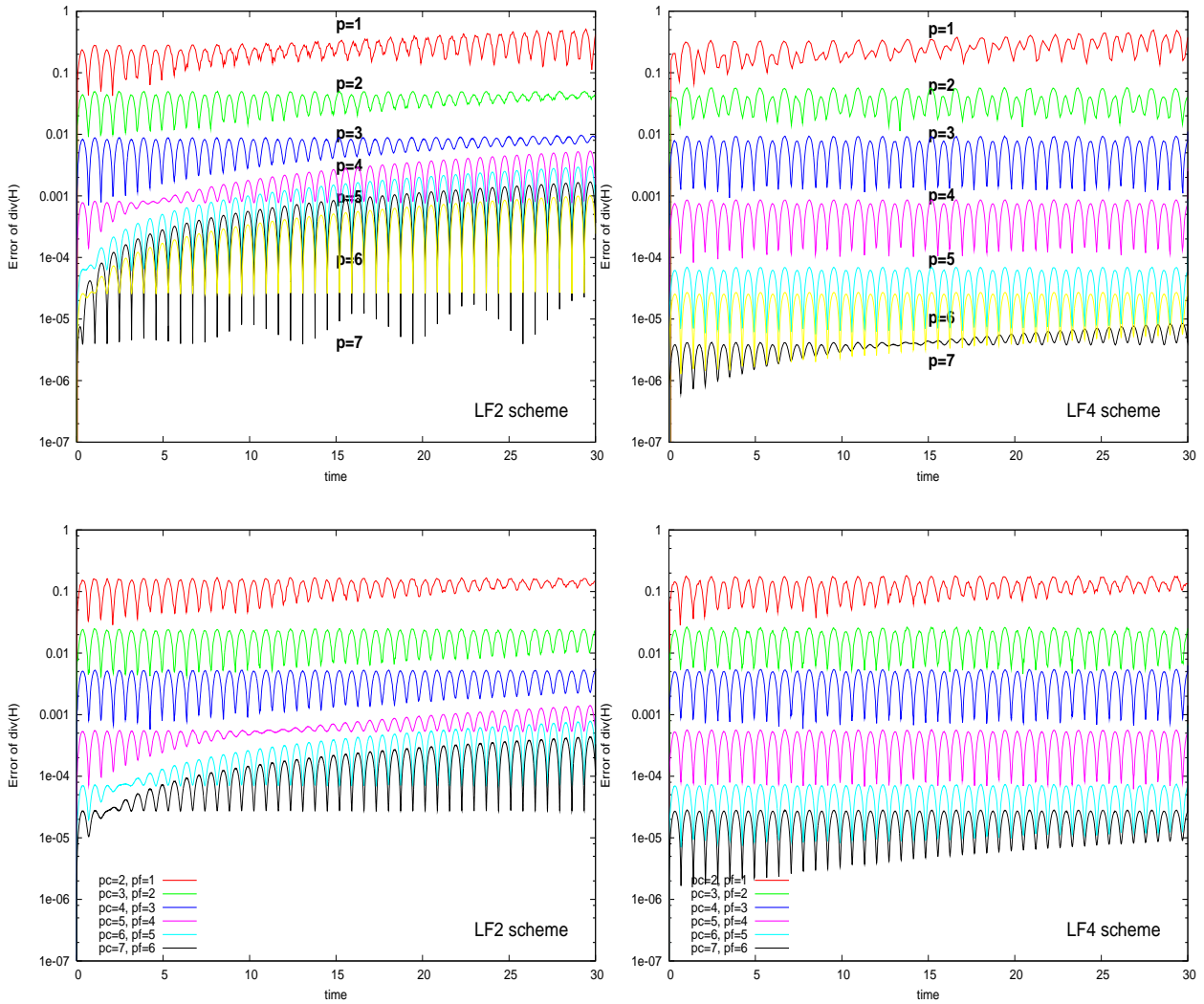


Figure 8: Global L^2 error of the divergence of \vec{H} as a function of time and p . $DGTD-\mathbb{P}_p$ (top) and $DGTD-\mathbb{P}_{p_c}:\mathbb{P}_{p_f}$ (bottom) methods using LF_2 (left) and LF_4 (right) schemes.

On Fig. 9 we show the numerical h - and p -convergence of the divergence of $\vec{\mathbf{H}}$ using the LF₂ and LF₄ schemes. Consistent with the theoretical result in Theorem 3.2, the divergence error vanishes spectrally as we increase the approximation order p . Corresponding asymptotic convergence orders of the divergence of $\vec{\mathbf{H}}$ are given in Tab. 7. One can observe that the convergence order is bounded by $N + 2$ contrary to what we have observed for the h -convergence of the DGTD methods which confirms that the estimate (50) is suboptimal and leaves room for improvement.

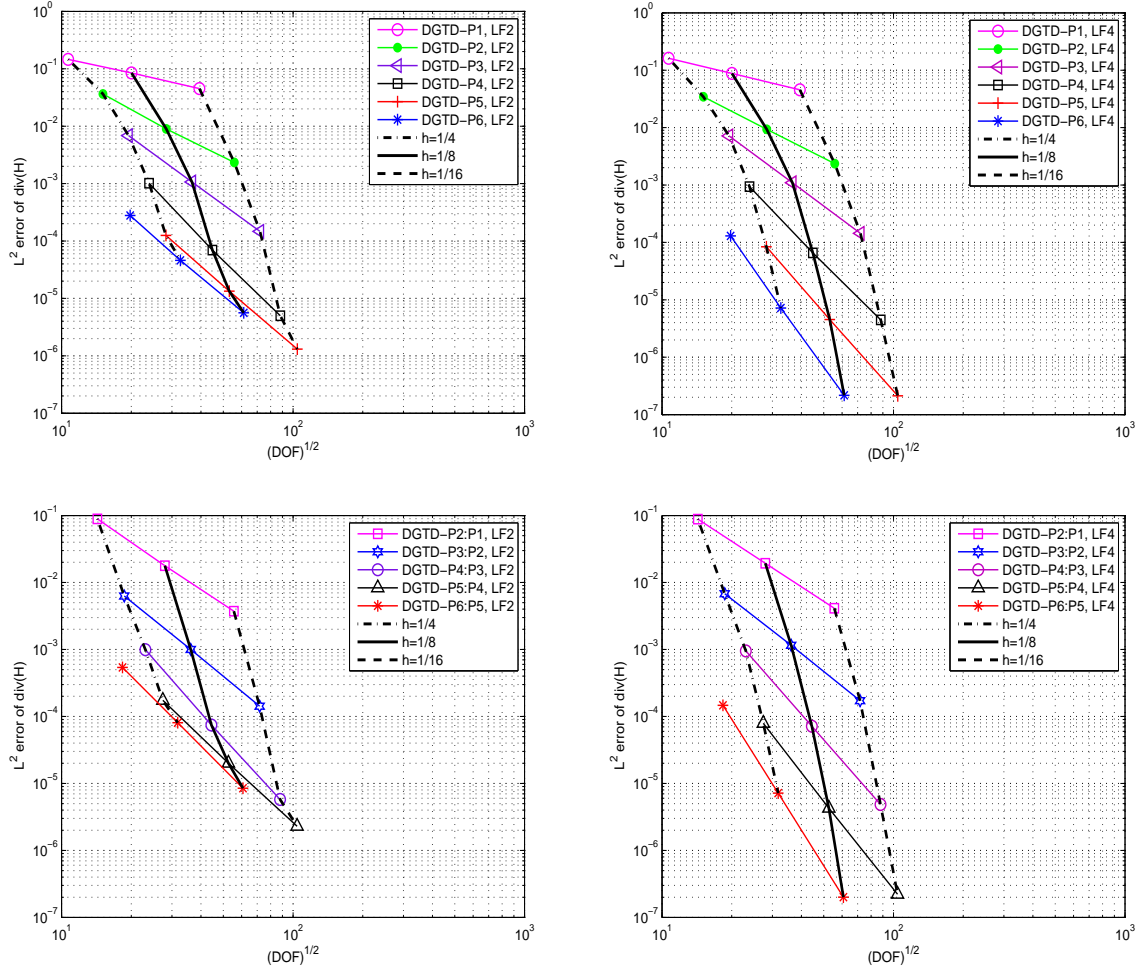


Figure 9: h - and p -convergence of the divergence of $\vec{\mathbf{H}}$.
 DGTD- \mathbb{P}_p (top) and DGTD- $\mathbb{P}_{p_c}:\mathbb{P}_{p_f}$ (bottom) methods.

Table 7: Asymptotic convergence orders of the divergence of $\vec{\mathbf{H}}$.

DGTD- \mathbb{P}_p method, $p =$	1	2	3	4	5	6
LF ₂ scheme	0.89	2.10	2.94	4.07	3.49	3.45
LF ₄ scheme	0.97	2.05	3.00	4.09	4.58	5.66
DGTD- $\mathbb{P}_{p_c}:\mathbb{P}_{p_f}$ method, $p_c:p_f =$	2:1	3:2	4:3	5:4	6:5	
LF ₂ scheme	2.33	2.81	3.84	3.24	3.46	
LF ₄ scheme	2.26	2.73	3.94	4.40	5.50	

5 Concluding remarks

The main purpose of this report has been to study both theoretically and numerically an arbitrarily high-order DGTD method for the discretization of the time-domain Maxwell equations on non-conforming simplicial meshes. The central element which distinguishes the current work from previous attempts to develop such DGTD methods is that a high-order leap-frog time integration scheme is adopted here instead of a high-order Runge-Kutta method. We have proved that the resulting DGTD method conserves a discrete equivalent of the electromagnetic energy and is stable under some CFL-type condition. Also, we have developed a complete, if not optimal, convergence theory. We have confirmed the results of the analysis thorough numerical experiments using an eigenmode problem in two space dimensions, illustrating the flexibility, versatility, and efficiency of the proposed arbitrarily high-order DGTD method.

References

- [1] I. Babuska and M. Suri. The *hp*-version of the finite element method with quasiuniform meshes. *RAIRO: M2AN*, 21(2):199–238, 1987.
- [2] M. Bernacki, L. Fezoui, S. Lanteri, and S. Piperno. Parallel unstructured mesh solvers for heterogeneous wave propagation problems. *Appl. Math. Model.*, 30(8):744–763, 2006.
- [3] M.H. Carpenter and C.A. Kennedy. Fourth-order 2N-storage Runge-Kutta schemes. Nasa-tm-109112, NASA Langley Research center, VA, 1994.
- [4] M.-H. Chen, B. Cockburn, and F. Reitich. High-order RKDG methods for computational electromagnetics. *J. Sci. Comput.*, 22(1):205–226, 2005.
- [5] O. Clatz, S. Lanteri, S. Oudot, J.-P. Pons, S. Piperno, G. Scarella, and J. Wiart. Modélisation numérique réaliste de l'exposition des tissus de la tête à un champ électromagnétique issu d'un téléphone mobile. In *13ème Colloque International et Exposition sur la Compatibilité Electromagnétique*, pages 377–397, Saint Malo, France, 2000.
- [6] G. Cohen, X. Ferrieres, and S. Pernet. A spatial high-order hexahedral discontinuous Galerkin method to solve Maxwell's equations in time domain. *J. Comp. Phys.*, 217:340–363, 2006.
- [7] H. Fahs. Numerical evaluation of a non-conforming discontinuous Galerkin method on triangular meshes for solving the time-domain Maxwell equations. Research Report 6311, INRIA, 2007. [Online]. Available: <http://hal.inria.fr/inria-00175738/>.
- [8] H. Fahs. Development of a *hp*-like discontinuous Galerkin time-domain method on non-conforming simplicial meshes for electromagnetic wave propagation. *Int. J. Numer. Anal. Model.*, to appear., 2008.
- [9] H. Fahs, L. Fezoui, S. Lanteri, and F. Rapetti. Preliminary investigation of a non-conforming discontinuous Galerkin method for solving the time domain Maxwell equations. *IEEE Trans. on Magnet.*, 44(6):1254–1257, 2008.
- [10] H. Fahs, S. Lanteri, and F. Rapetti. Etude de stabilité d'une méthode Galerkin discontinu pour la résolution numérique des équations de Maxwell 2D en domaine temporel sur des maillages triangulaires non-conformes. Research Report 6023, INRIA, Juillet 2006. [Online]. Available: <http://hal.inria.fr/inria-00114537/>.
- [11] H. Fahs, S. Lanteri, and F. Rapetti. A *hp*-like discontinuous Galerkin method for solving the 2D time-domain Maxwell's equations on non-conforming locally refined triangular meshes. Research Report 6162, INRIA, 2007. [Online]. Available: <http://hal.inria.fr/inria-00140783/>.

-
- [12] H. Fahs, S. Lanteri, and F. Rapetti. Development of a non-conforming discontinuous Galerkin method on simplex meshes for electromagnetic wave propagation. In M. Hogge, R. Van Keer, L. Noels, L. Stainier, J.-P. Ponthot, J.-F. Remacle, and E. Dick, editors, *4th Int. Conf. on Advanced Computational Methods in Engineering*. ACOMEN, 26-28 May, Liège, Belgium 2008. 10 pages.
- [13] J. Fang. *Time domain finite difference computation for Maxwell's equations*. PhD thesis, Univ. of Calif, Berkeley, 1989.
- [14] L. Fezoui, S. Lanteri, S. Lohrengel, and S. Piperno. Convergence and stability of a discontinuous Galerkin time-domain method for the heterogeneous Maxwell equations on unstructured meshes. *ESAIM: Math. Model. and Numer. Anal.*, 39(6):1149–1176, 2005.
- [15] J.S. Hesthaven and T. Warburton. Nodal high-order methods on unstructured grids. I. Time-domain solution of Maxwell's equations. *J. Comput. Phys.*, 181:186–221, 2002.
- [16] A. Kanevsky, M.H. Carpenter, D. Gottlieb, and J.S. Hesthaven. Application of implicit-explicit high-order Runge-Kutta methods to discontinuous Galerkin schemes. *J. Comput. Phys.*, 225(2):1753–1781, 2007.
- [17] T. Lu, P. Zhang, and W. Cai. Discontinuous Galerkin methods for dispersive and lossy Maxwell's equations and PML boundary conditions. *J. Comput. Phys.*, 200:549–580, 2004.
- [18] P. Monk and J. Richter. A discontinuous Galerkin method for linear symmetric hyperbolic systems in inhomogeneous media. *SIAM J. Sci. Comput.*, 22(1):433–477, 2005.
- [19] M. Remaki. A new finite volume scheme for solving Maxwell system. Technical Report 3725, INRIA, July 1999.
- [20] D. Sármany, M.A. Botchev, and J.J.W. van der Vegt. Dispersion and dissipation error in high-order Runge-Kutta discontinuous Galerkin discretisations of the Maxwell equations. *J. Sci. Comput.*, 33(1):47–74, 2007.
- [21] CH. Schwab. *p- and hp-finite element methods. Theory and applications to solid and fluid mechanics*. Oxford University Press, Oxford, UK, 1998.
- [22] H. Spachmann, R. Schuhmann, and T. Weiland. High order explicit time integration schemes for Maxwell's equations. *Int. J. Numer. Model.*, 15(6):419–437, 2002.
- [23] J. Tuomela. Fourth-order schemes for the wave equation, Maxwell's equations, and linearized elastodynamic equations. *Numerical Methods for PDEs*, 10(1):33–63, 1994.
- [24] T. Warburton and J.S. Hesthaven. On the constants in *hp*-finite element trace inequalities. *Comput. Meth. Appl. Mech. Engng.*, 192:2765–2773, 2003.
- [25] J.L. Young. High-order, leapfrog methodology for the temporally dependent Maxwell's equations. *Radio Science*, 36(1):9–17, 2001.



Centre de recherche INRIA Sophia Antipolis – Méditerranée
2004, route des Lucioles - BP 93 - 06902 Sophia Antipolis Cedex (France)

Centre de recherche INRIA Bordeaux – Sud Ouest : Domaine Universitaire - 351, cours de la Libération - 33405 Talence Cedex
Centre de recherche INRIA Grenoble – Rhône-Alpes : 655, avenue de l'Europe - 38334 Montbonnot Saint-Ismier
Centre de recherche INRIA Lille – Nord Europe : Parc Scientifique de la Haute Borne - 40, avenue Halley - 59650 Villeneuve d'Ascq
Centre de recherche INRIA Nancy – Grand Est : LORIA, Technopôle de Nancy-Brabois - Campus scientifique
615, rue du Jardin Botanique - BP 101 - 54602 Villers-lès-Nancy Cedex
Centre de recherche INRIA Paris – Rocquencourt : Domaine de Voluceau - Rocquencourt - BP 105 - 78153 Le Chesnay Cedex
Centre de recherche INRIA Rennes – Bretagne Atlantique : IRISA, Campus universitaire de Beaulieu - 35042 Rennes Cedex
Centre de recherche INRIA Saclay – Île-de-France : Parc Orsay Université - ZAC des Vignes : 4, rue Jacques Monod - 91893 Orsay Cedex

Éditeur
INRIA - Domaine de Voluceau - Rocquencourt, BP 105 - 78153 Le Chesnay Cedex (France)
<http://www.inria.fr>
ISSN 0249-6399